Aalto University
School of Science
Degree Programme of Engineering Physics and Mathematics

Eelis Solala

Dioxygen adsorption and dissociation on fullerenes - a computational study

Master's Thesis
Espoo, 13.6.2014

Supervisor: professor Esko Kauppinen
Instructors: Stefan Taubert PhD
professor Kari Laasonen

Aalto University
School of Science
Degree Programme of Engineering Physics and Mathematics

ABSTRACT OF
MASTER'S THESIS

Author:	Eelis Solala
Title:	
Dioxygen adsorption and dissociation on fullerenes - a computational study	

Date:	13.6.2014	**Pages:**	vii + 75
Professorship:	Physics	**Code:**	Tfy-3

Supervisor:	professor Esko Kauppinen
Instructors:	Stefan Taubert PhD
	professor Kari Laasonen

In this thesis, the adsorption and dissociation of oxygen molecule on different fullerenes are studied by calculating the adsorption and dissociation energies for different reaction paths. In addition, the activation energies for the dissociation reaction of the adsorbed oxygen molecule are calculated for selected reaction paths. All calculations are based on the density functional theory (DFT), and the calculations are carried out with the CP2K program.

The studied fullerenes are C60, C59N, C180, and C179N. For each of these, the effects of charging on the bond lengths and reaction energies are studied. Studying charged fullerenes may give some insight to endohedral metallofullerenes, as the carbon atoms in those systems are also negatively charged. One of the central goals of this thesis is to understand the effects of the fullerene charge, nitrogen doping, and the size of the fullerene on the adsorption, dissociation, and activation energies for the dissociation reaction.

It was found that the size, charge, and presence of nitrogen on the fullerene all affect the reaction energies. Both extra charge and nitrogen doping make both the adsorption and dissociation of the oxygen molecule more energetically favourable compared to a free oxygen molecule. Increasing the size of the fullerene has the opposite effect. Besides these three parameters, the adsorption site of the oxygen molecule on the fullerene also has a large effect on the reaction energies. It was also seen that both extra charge and nitrogen lower the activation energies for the dissociation of the adsorbed oxygen molecule. The size of the fullerene has only a weak effect on the activation energies.

Keywords:	Density functional theory, DFT, fullerenes, adsorption, dissociation
Language:	English

Tekijä:	Eelis Solala		
Työn nimi:			
Hapen adsorptio ja hajoaminen fullereeneilla			
Päiväys:	13.6.2014	**Sivumäärä:**	vii + 75
Professuuri:	Fysiikka	**Koodi:**	Tfy-3
Valvoja:	professori Esko Kauppinen		
Ohjaajat:	FT Stefan Taubert		
	professori Kari Laasonen		

Tässä työssä tutkitaan happimolekyylin adsorptiota ja dissosiaatiota erilaisten fullereenien pinnoilla. Happimolekyylin eri reaktiopoluille lasketaan adsorptio- ja dissosiaatioenergiat. Tämän lisäksi tarkastellaan muutamalla valitulla polulla myös aktivaatioenergiaa happimolekyylin adsorboituneen ja dissosioituneen tilan välillä. Työssä käytetään tiheysfunktionaaliteoriaa (DFT), jonka laskujen suorittamiseen käytetään CP2K-nimistä ohjelmistoa.

Työssä tutkittavat fullereenit ovat C_{60} ja $C_{59}N$ sekä C_{180} ja $C_{179}N$. Kussakin analysoidussa tapauksessa tarkasteltiin fullereenin varauksen vaikutusta eri atomien välisten sidosten pituuksiin ja reaktioenergioihin. Varattujen fullereenien tutkiminen voi tuoda lisätietoa myös metallitäytteisistä fullereeneista, sillä mikäli fullereenin sisällä on metalliatomeja, jotka luovuttavat elektroneja sille, sen varaus muuttuu negatiiviseksi kuten tässäkin tutkituilla fullereeneilla. Työn yhtenä keskeisenä tavoitteena onkin ymmärtää fullereenin sähkövarauksen ja yhden hiiliatomin korvaamisen typpiatomilla vaikutuksia hapen adsorptio- ja dissosiaatioenergioihin sekä aktivaatioenergioihin adsorboituneen ja dissosioituneen konfiguraation välillä.

Tehtyjen laskujen perusteella havaittiin, että fullereenin koko, varaus, ja typenlisäys systeemiin vaikuttavat reaktioenergioihin. Typpilisäys ja fullereenin varaus siirtävät happimolekyylin adsorptio- ja dissosiaatioreaktioiden tasapainotilaa reaktiotuotteiden suuntaan. Sen sijaan fullereenin koon kasvattaminen vaikutti päinvastaiseen suuntaan. Lisäksi havaittiin, että sillä mihin fullereenin kohtaan happimolekyyli kiinnittyy on huomattava vaikutus reaktioenergioihin. Sekä typpidouppaus että varaus myös pienentävät aktivaatioenergiaa adsorboituneen happimolekyylin dissosiaatioreaktiossa, eli ne nopeuttavat happimolekyylin hajoamista. Fullereenin koon kasvattaminen puolestaan vaikuttaa aktivaatioenergiaan korkeintaan heikosti.

Asiasanat:	tiheysfunktionaaliteoria, DFT, fullereenit, adsorptio, dissosiaatio
Kieli:	englanti

Acknowledgements

Abbreviations and Acronyms

C_{60}	$(C_{60}$-$I_h)$[5-6]fullerene
DFT	Density functional theory
GGA	generalized gradient approximation
GTH	Goedecker-Teter-Hutter
GPW	Gaussian and plane wave method
HH	hexagon-hexagon
HP	hexagon-pentagon
IPR	isolated pentagon rule
LDA	local density approximation
LSD	local spin density approximation
MEP	minimum energy path
NEB	nudged elastic band method
PBE	Perdew-Burke-Ernzerhof
SOM	Self-organizing map

Contents

Chapter 1

Introduction

Carbon nanomaterials have become a topic of great scientific interest recently. A lot of research is done about fullerenes, carbon nanotubes, as well as graphene. Finding possible applications for these materials is also of great interest. In this thesis several fullerenes are studied.

One suggested application for fullerenes and fullerene-based materials has been to use them as catalysts for fuel cells [1]. Breaking a dioxygen molecule to separate oxygens is often the step that limits the efficiency of fuel cells. That is why it is interesting to see what properties affect this process.

In this thesis the important question is what affects the oxygen reduction reactions on fullerenes. The scientific interest is the effect of size of the system, presence of nitrogen, and the charge of the system to the energetics of dioxygen adsorption and dissociation. The case of charged fullerenes is interesting because in endohedral metallo-fullerenes, a net charge on the fullerene part has been observed.

This thesis begins with a short introduction to fuel cells, catalysis and fullerenes. After that, a brief description of the methods used in this thesis is given, beginning with density functional theory, then proceeding with nudged elastic band method, and the definition of Bader charge. A brief description of self-organizing maps is also given. This is followed by results: optimized geometries of the fullerenes obtained via density functional theoretical calculations. After the geometries of the fullerenes are presented, the adsorption of dioxygen molecules, and the related quantities are presented. Adsorption configurations are followed by related oxygen dissociation configurations. After these results have been presented, the energetics of different reaction pathways are briefly summarized. This is followed by discussion of the effects of the size of the fullerene, presence of nitrogen, and the charge of the system.

Chapter 2

Background

In this chapter the background of this thesis is discussed. Fuel cells are discussed briefly. Catalysis is then discussed and in particular how it relates to the fuel cell reactions. Then the fullerenes are discussed.

2.1 Fuel cells

A fuel cell is a device where chemical energy is converted into electricity without any additional energy conversions [2, 3]. A fuel cell consists of three main parts: anode, cathode and electrolyte. A common fuel in fuel cells is hydrogen.
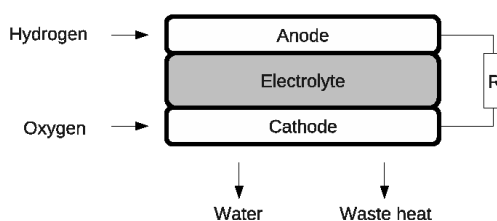
Figure 2.1: A schematic of a fuel cell. R stands for the load of the outer circuit.

Figure 2.1 shows a schematic representation of the structure and operation of the fuel cell. Hydrogen is lead to the anode, and oxygen is lead to the cathode.

There are several partial processes that take part in a fuel cell [4]. First, we have a reaction at the anode:

$$2H_2(g) \rightarrow 4H^+ + 4e^-. \tag{2.1}$$

The reaction at the cathode is:

$$O_2(g) + 4H^+ + 4e^- \rightarrow 2H_2O(l). \tag{2.2}$$
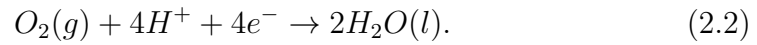
Combining the anode and cathode partial reactions we get the total reaction [5]:

$$2H_2(g) + O_2(g) \rightarrow 2H_2O(l). \tag{2.3}$$
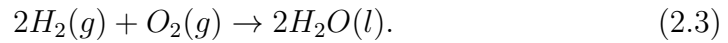
The oxygen reduction reaction at the cathode plays a key role in a fuel cell [6]. It is therefore very important to have it happen as efficiently as possible [7].

2.2 Catalysis

A catalyst is a substance that speeds up a reaction without changing the overall standard Gibbs energy change ΔG in the reaction [8]. Unlike other reagents in a chemical reaction, the catalyst is not consumed in the reaction. In other words, there is the same amount of catalyst before and after the reaction.

Catalysis is often divided into two categories, homogeneous catalysis and heterogeneous catalysis. In homogeneous catalysis the catalyst is in the same phase as the reactants, whereas in heterogeneous catalysis the phase of the catalyst is different than the phase of the reactants. [9, 10]
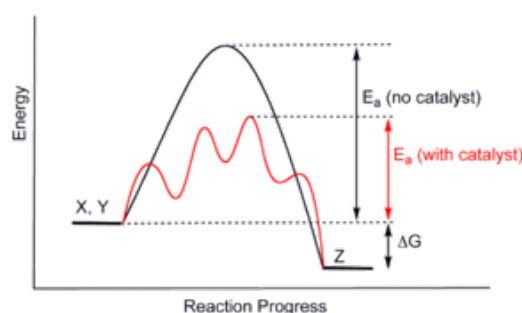
Figure 2.2: A potential energy diagram showing the effect of the catalyst [3]. We see that the activation energy E_a is a lot smaller with the catalyst than without. We also see that the free energy change ΔG stays the same with and without the catalyst.

Figure 2.2 shows the effect the catalyst has on a reaction. We see that the activation energy is lower with the catalyst than without it. We also observe that the reaction energy ΔG stays the same in the reaction with and without the catalyst. We also see that the energy landscape with the catalyst is more complicated than without the catalyst. This is because the catalyst takes part in the reaction and the local energy minima among the path correspond to intermediate states.

Lowering the activation energy can lead to a faster reaction rate. According to the Arrhenius equation [11, 12] the rate constant k of a reaction depends on the activation energy E_a:

$$k = Ae^{-\frac{E_a}{k_B T}}, \tag{2.4}$$

where A is a prefactor, k_B is the Boltzmann constant and T is the temperature. Assuming that the prefactor term stays the same, we see that lowering

the activation energy leads to considerable speed-ups in the reaction speed. The prefactor A has a weak temperature dependence [13, 14]. In this thesis the temperature is not taken into account.

It can be seen that lowering the activation energy leads to higher reaction rates. However, this is not everything we want from a catalyst. We often have many competing reactions that are happening at the same time. An ideal catalyst would only speed-up the output of desirable end-products. In ideal catalyst is therefore also selective [15].

In a fuel cell application the production of hydrogen peroxide:

$$2H^+ + 2e^- + O_2 \rightarrow H_2O_2 \tag{2.5}$$
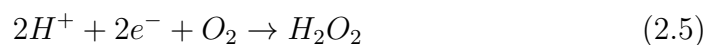
is not desirable, because it is known to contribute to the chemical degradation of fuel cells [16]. It can now be seen that for fuel cell applications we want such catalysts that the oxygen dissociation gets faster, but the hydrogen peroxide formation does not.

2.3 Fullerenes

A fullerene is a hollow spherical molecule composed of carbon. First ever fullerene to be found was the buckminsterfullerene consisting of 60 carbon atoms. A stable 60 carbon atom molecule was predicted theoretically in the 1970s [17]. The buckminsterfullerene was experimentally observed in the 1980s [17, 18].

Fullerenes follow Euler's formula for polyhedra:

$$v + f = e + 2, \tag{2.6}$$

where v is the number of vertices, e is the number of edges and f is the number of faces. In this case v is the number of atoms and e is the number of bonds between the atoms. The number of faces f can also be written as:

$$f = \frac{5}{6}p + h + 2, \tag{2.7}$$

where p is the number of pentagons and h is the number of hexagons. It can further be shown, that for a cage of v atoms, it must contain 12 pentagons and $(\frac{v}{2} - 10)$ hexagons. This means that if there are 60 atoms in a fullerene, there are 12 pentagons and 20 hexagons in it.

When talking about the 60 atom fullerene, it should be remembered that the 12 pentagons and 20 hexagons may form 1812 topologically different isomers. It turns out that the one with most symmetry out of all the possible structures is the most stable of them.

The number of topologically different fullerenes as a function of number of atoms grows quite rapidly [19]. Table 2.1 shows the number of fullerene isomers as a function of number of atoms on the fullerene molecule. We see a combinatoric explosion of the numbers.

n	20	22	24	26	28	30	40	60	80	100
isomers	1	0	1	1	2	3	40	1812	31924	285913

Table 2.1: Number of topologically different isomers as a function of number of atoms.

For larger fullerenes it is energetically favourable for the pentagons to be located only next to hexagons. This rule is called the isolated pentagon rule (IPR). However, it should be known that for example in the case of charged fullerene, or endohedral or exohedral system, the IPR system might not be the most stable form. Because of the large number of possible isomers, it is very important to have an efficient way to find the most stable isomers

without going through them all. The IPR is often a good place to start
looking.

Fullerenes can always be represented as a planar graph. A Schlegel di-
agram of the C_{60} obeying the isolated pentagon rule can be seen in figure
2.3.
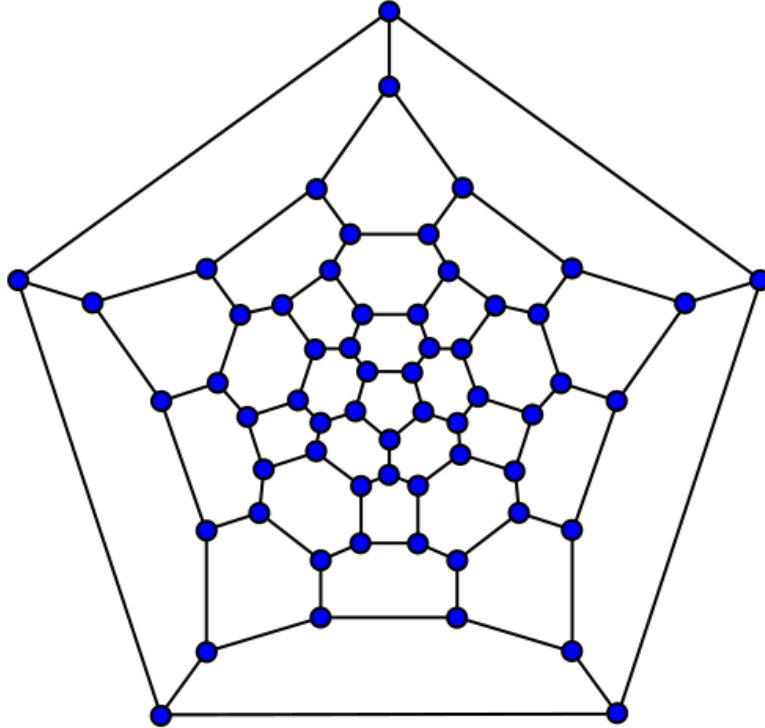
Figure 2.3:   A Schlegel diagram of the isolated pentagon C_{60}. Every node
corresponds to a carbon atom.

A common way for visualizing carbon nanotubes is thinking of them
as rolled up graphene sheets [20]. There is also a similar approach to the
fullerenes [21]. In this approach the starting point is the honeycomb lattice
of carbon. On the lattice there is a pentagon defect and it removes a sec-
tion of lattice, figure 2.4. This change of a hexagon to a pentagon causes a
distortion on the lattice.

We then place a second pentagonal defect on the lattice. The location
of the second defect is specified by the lattice vectors $\vec{a}$ and $\vec{b}$ and a pair of
indexes (m, n). Figure 2.5 shows an example of the location of the second
defect with indexes $(m, n) = (2, 1)$.

A fullerene with an icosahedral symmetry is fully specified by the pair
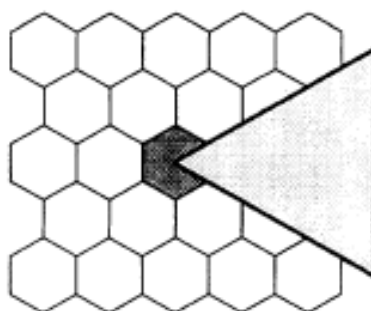
Figure 2.4: Location of the pentagon defect on the hexagonal lattice. The area marked by the triangle is removed when hexagon is turned to a pentagon.
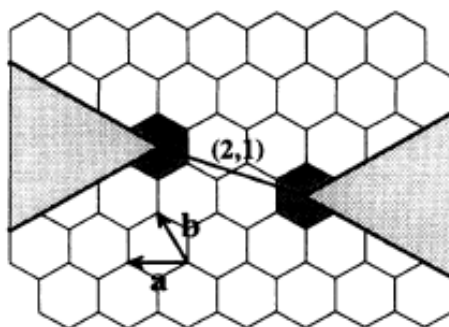
Figure 2.5: The location of the second pentagonal defect on a hexagonal lattice. In this case the second defect is specified by $(m, n) = (2, 1)$.

(m, n). This symmetry is obtained by placing five pentagons on 60° intervals. Figure 2.6 shows the full construction of the $(2, 1)$ fullerene on the honeycomb lattice.

A fullerene described by (m, n) contains $20(m^2 + mn + n^2)$ carbon atoms. For example the 60 atom fullerene is given by $(1, 1)$. This method of obtaining fullerenes from graphene sheet can also be generalized to fullerenes with no icosahedral symmetries.
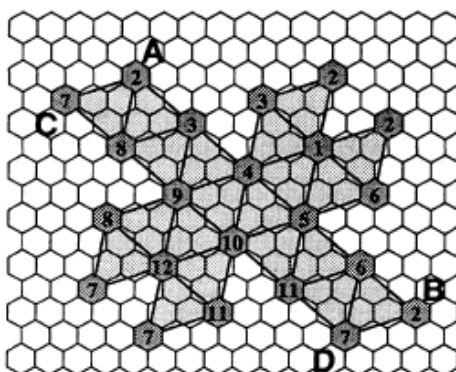
Figure 2.6: The locations of all pentagon defects in the $(m, n) = (2, 1)$ fullerene. Sites with the same number are taken to be taken the same. This results in a spherical structure. This results in an icosahedral 140 atom fullerene. Every number on the picture corresponds to a site where a hexagon is transformed to a pentagon.

Both the graph theoretical and the geometrical approach give some insight to the structure of fullerenes. It is also good to see how they are synthesized. There are several possible ways to produce fullerenes. A common method for producing fullerenes is the arc vaporization method [22], sometimes referred to as the Krätschmer-Huffman method.
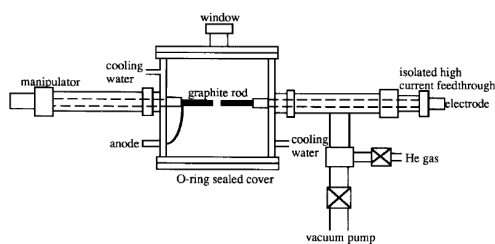
Figure 2.7: A schematic illustration of the apparatus for producing fullerenes with the arc vaporization method.

A schematic of the apparatus used in the arc vaporization method can be seen in figure 2.7. At first the reaction chamber is turned into a vacuum. After that, the chamber is filled with a helium atmosphere. Then a large current is lead through the graphite rods. This leads to the formation of fullerene containing soot on the sides of the chamber. The fullerene molecules

will then have to be separated from the soot.
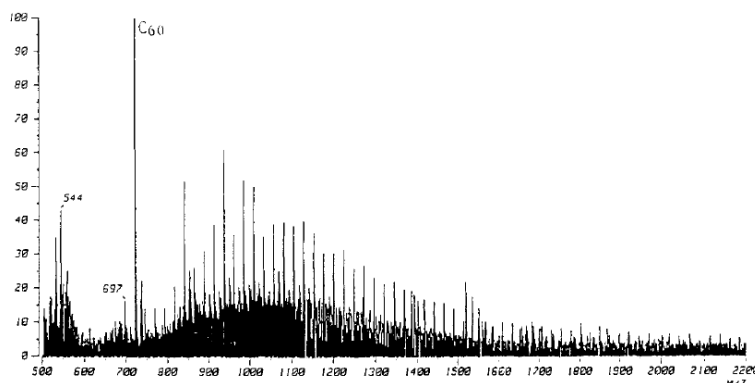
Figure 2.8:   Mass spectrum of soot obtained with the arc vaporization method. We see that a large number of different carbon products are produced. The intensity spike corresponding to the 60 atom fullerene has been scaled to 100.

Figure 2.8 shows the mass spectrum of a sample analyzed by the arc vaporization method. There are many spikes in the spectrum, each corresponding to a different carbon product.

There are also fullerenes, in which one or many carbon atoms have been replaced with atoms of other elements. The other elements observed have been for example nitrogen [23], boron [24, 25], arsenic, germanium [26] and silicon [27, 28]

Besides the fullerenes where a carbon atom has been replaced with an atom of another element there are also other fullerene based materials. An example of these would be fullerenes with additional atoms, ions or clusters inside of them. These endohedral fullerenes are often quite interesting. For example if there are metal atoms inside the carbon cage, the electrons from the metal atoms have the tendency to move to the fullerene making it negatively charged [29, 30].

Possible future uses of fullerenes include for example lubricants [31–34], drug delivery [35–38] and catalysis [39–44].

Chapter 3

Methods

In this chapter the methodology of the thesis is explained. First thing that is discussed is the density functional theory and how it is used in calculations. This is followed by an introduction to the Nudged Elastic Band method used for studying the transition states in processes. Bader charge is then presented as a definition of a partial charge. The chapter concludes with a short introduction to self-organizing maps.

3.1 Density functional theory

The density functional theory is a quantum mechanical tool for obtaining the physical properties of a system from the electron density of the ground state of the system.

In the Born-Oppenheimer approximation of a many atom system we have the Hamiltonian H [45]:

$$H = T + V + U, \qquad (3.1)$$

where T is the kinetic energy:

$$T = -\frac{1}{2} \sum_i \nabla_i^2, \qquad (3.2)$$

U is the interaction energy:

$$U = \frac{1}{2} \sum_{i,j} \frac{1}{|r_i - r_j|} \qquad (3.3)$$

and V is the external potential:

$$V = \sum_i V(r_i), \qquad (3.4)$$

where r_i is the position of electron i.

First Hohenberg-Kohn theorem (1) states that the ground state density $n(r)$ defines, up to a constant, the external potential $V(r)$. Since the density n also defines the particle number N, it also defines the full Hamiltonian H. Now, for a given potential $V(r)$ it is possible to write an energy functional $E_{V(r)}$:

$$E_{V(r)} = \int V(r)n(r)dr + F[n(r)], \qquad (3.5)$$

where $F[n(r)]$ is defined as:

$$F[n(r)] = \langle \Psi[n(r)]| \, T + U \, |\Psi[n(r)]\rangle . \qquad (3.6)$$

Variational principle says, that for all $n(r)$ it holds that:

$$E_0 = E_{V(r)}[n_0(r)] \leq E_{V(r)}[n(r)], \qquad (3.7)$$

where E_0 and n_0 are the energy and the density of the ground state.

$F[n]$ may now be written in another way:

$$F[n(r)] = T_s[n(r)] + \frac{1}{2} \int \frac{n(r)n(r')}{|r - r'|} dr dr' + E_{xc}[n(r)], \qquad (3.8)$$

where $T_s[n]$ is the kinetic energy of a non-interacting system with density n and the second term is the classical electron electron interaction term. This equation is taken as the definition of the exchange correlation energy E_{xc}.

We now obtain the Kohn-Sham equations for the energy $E_V[n]$:

$$(-\frac{\nabla^2}{2} + V(r) + \int \frac{n(r')dr'}{|r - r'|} + V_{xc})\phi_i = \epsilon_i \phi_i, \qquad (3.9)$$

or in an alternative form:

$$(-\frac{\nabla^2}{2} + V_{eff}(r))\phi_i = \epsilon_i \phi_i, \qquad (3.10)$$

where:

$$n(r) = \sum_i |\phi_i(r)|^2 \qquad (3.11)$$

and:

$$V_{xc}(r) = \frac{\delta E_{xc}[n]}{\delta n}. \qquad (3.12)$$

and the effective potential V_{eff} is:

$$V_{eff}(r) = V(r) + \int \frac{n(r')dr'}{|r - r'|} + V_{xc}. \qquad (3.13)$$

The eigenvalues ϵ_i and eigenfunctions ϕ_i in equation 3.9 have no direct physical interpretation.

We now have one more equation for the ground state energy E_0:

$$E_0 = \sum_i \epsilon_i - \frac{1}{2} \int \frac{n(r)n(r')drdr'}{|r-r'|} - \int V_{xc}(r)n(r)dr + E_{xc}[n(r)]. \quad (3.14)$$

This equation is in principle exact. The only errors in it come from the approximations in E_{xc}. In practice it is difficult to find good expressions for $E_{xc}[n(r)]$. There are several widely used approximations. The simplest of them is the local density approximation (LDA):

$$E_{xc}^{LDA}[n(r)] = \int \epsilon_{xc}(n(r))n(r)dr, \quad (3.15)$$

where $\epsilon_{xc}(n)$ is the exchange-correlation energy per particle in uniform interacting electron gas with density of n. This quantity is quite well known.

The second widely used family of functionals are the generalized gradient approximations (GGA) :

$$E_{xc}^{GGA} = \int f(n(r), \nabla n(r))dr, \quad (3.16)$$

where f is some function of two variables fitting for the problem. It is worth noticing that the parameters in LDA have a physical meaning, but the parameters in GGA don't need to have it.

In figure 3.1 there is a flowchart of what is done in a DFT calculation. From the initial guess of the density, we first solve the effective potential. After the effective potential is known, the Kohn-Sham equations related to it are solved. After the Kohn-Sham equations have been solved, we can get the new density. This procedure is repeated until the density converges.
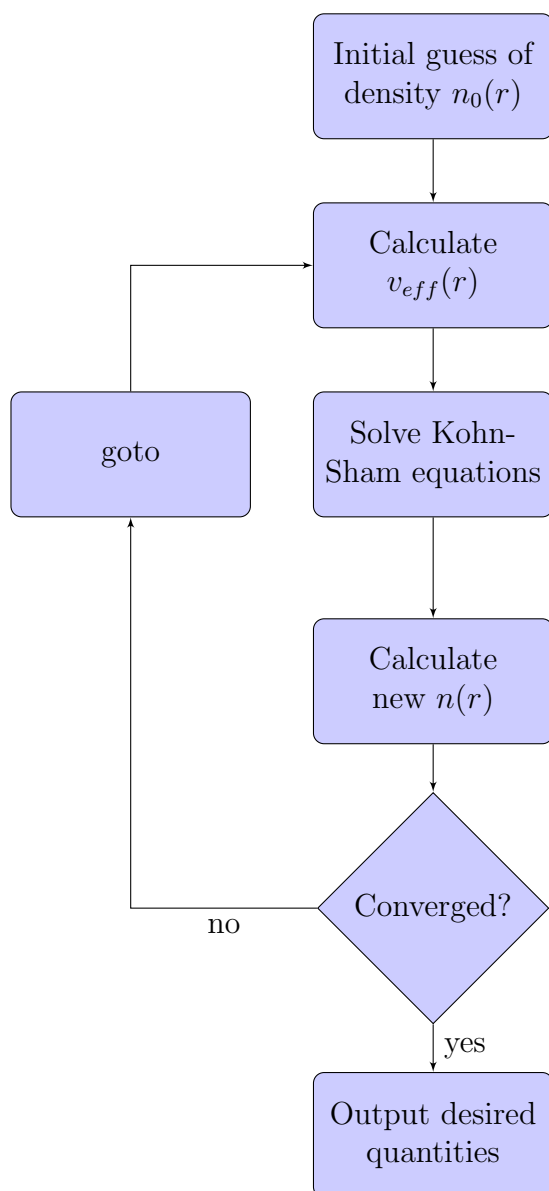
Figure 3.1: A flowchart of what happens in a DFT calculation

3.1.1   Hohenberg-Kohn theorems

There are two very important theorems in the background of the density functional theory.

Theorem 1 *The external potential $V(\vec{r})$ is, up to a constant, a unique functional of the density $n(\vec{r})$.*

Assume we have two external potentials v_1 and v_2 that differ by more than a constant that give the same ground state density $n_0(r)$. Therefore there are two different Hamiltonians H_1 and H_2 that have the ground states Ψ_1 and Ψ_2 that give the same ground state density $n_0(r)$.

Now we have:

$$E_1^0 = \langle \Psi_1 | H_1 | \Psi_1 \rangle. \tag{3.17}$$

By the variational principle it holds that:

$$E_1^0 < \langle \Psi_2 | H_1 | \Psi_2 \rangle, \tag{3.18}$$

where the equality cannot hold as Ψ_1 and Ψ_2 were assumed to be different. It also holds that:

$$H_1 = H_2 + H_1 - H_2. \tag{3.19}$$

From which we get:

$$E_1^0 < E_2^0 + \int n_0(r)(v_1(r) - v_2(r))dr. \tag{3.20}$$

A similar inequality holds also after changing the order of 1 and 2:

$$E_2^0 < E_1^0 + \int n_0(r)(v_2(r) - v_1(r))dr. \tag{3.21}$$

Summing the two inequalities we obtain:

$$E_1^0 + E_2^0 < E_1^0 + E_2^0, \tag{3.22}$$

which is a contradiction. This proves theorem 1.

Theorem 2 *The groundstate energy can be obtained variationally: the density that minimises the total energy is the exact groundstate density.*

By theorem 1 the density $n(r)$ defines $V(r)$. The density $n(r)$ also defines the particle number N. The density $n(r)$ therefore defines the system Hamiltonian H and also the ground state wave function Ψ.

The expectation values of $\hat{F}$ is also therefore a functional of $n(r)$:

$$F[n(r)] = \langle \Psi[n(r)] | \hat{F} | \Psi[n(r)] \rangle \tag{3.23}$$

Now:

$$E[n(r)] = \langle \Psi[n(r)] | \hat{F} + V | \Psi[n(r)] \rangle . \tag{3.24}$$

Another energy functional for a different state Ψ' can be defined:

$$E_V[n'(r)] = \int n'(r) V(r) dr + F[n'(r)] \tag{3.25}$$

From variational principle we obtain:

$$\langle \Psi' | \hat{F} | \Psi' \rangle + \langle \Psi' | V | \Psi' \rangle > \langle \Psi | \hat{F} | \Psi \rangle + \langle \Psi | V | \Psi \rangle , \tag{3.26}$$

where Ψ is the ground state wavefunction. Now combining we obtain:

$$E_V[n'(r)] > E_V[n(r)]. \tag{3.27}$$

That is to say, densities different from the ground state density have higher energies. This means that the ground state density gives the global minimum of the energy functional.

3.1.2   Gaussian and plane waves method

In the Gaussian and plane waves method (GPW) the energy functional $E[n]$ is written as a sum of five terms [46]:

$$E[n] = E^T[n] + E^V[n] + E^H[n] + E^{XC} + E^{II}, \tag{3.28}$$

where E^T is the kinetic energy, E^V is the electron-core interaction, E^H is the electronic Hartree energy, E^{XC} is the exchange correlation energy and E^{II} is ion-ion interaction energy.

Assume now, that we have a set of functions ϕ_i such that:

$$\phi_i = \sum_j d_{ij} g_j(\vec{r}), \tag{3.29}$$

where $g_j(r)$ are Gaussian functions. The density n can now be written as a sum:

$$n(\vec{r}) = \sum_{ij} P^{ij} \phi_i \phi_j, \tag{3.30}$$

where P^{ij} is an element of the density matrix.

We can also define an auxiliary density $\tilde{n}(r)$:

$$\tilde{n}(\vec{r}) = \frac{1}{V} = \sum_{\vec{k}} \tilde{n}(\vec{k}) e^{i\vec{k}\cdot\vec{r}}, \tag{3.31}$$

where V is the volume of the unit cell and $\vec{k}$ are the reciprocal lattice vectors. The coefficients $\tilde{\vec{k}}$ are such that:

$$n(\vec{r}) = \tilde{n}(\vec{r}), \tag{3.32}$$

when $\vec{r}$ is in the unit cell. We now have two possible representations for the density in the unit cell.

It is now possible to write the terms in the energy functional more explicitly. The kinetic energy functional E^T may be written as:

$$E^T[n] = \sum_{ij} P^{ij} \langle \phi_i(\vec{r})| - \frac{\nabla^2}{2} |\phi_j(\vec{r})\rangle. \tag{3.33}$$

It is possible to divide the electron-core interaction term E^V to two parts:

$$E^V[n] = \sum_{ij} P^{ij} \langle \phi_i(\vec{r})| V^{PP}_{local}(\vec{r}) |\phi_j(\vec{r})\rangle + \sum_{ij} P^{ij} \langle \phi_i(\vec{r})| V^{PP}_{non-local}(\vec{r}, \vec{r'}) \left|\phi_j(\vec{r'})\right\rangle, \tag{3.34}$$

where the electron-core interaction has been divided into local and non-local parts. The second change that has been done was going from the real potential V to the pseudopotentials V^{PP}.

The Hartree energy E^H is calculated with the auxiliary density:

$$E^H[n] = 2\pi V \sum_{\vec{k}} \frac{\tilde{n}^*(\vec{k})\tilde{n}(\vec{k})}{k^2}, \tag{3.35}$$

where V is the volume of the unit cell.

Exchange-correlation energy E^{xc} is calculated with suitable exchange correlation functional ϵ^{xc}:

$$E^{xc} = \int \epsilon^{xc} dr. \tag{3.36}$$

The ion-ion interaction E^{II} is:

$$E^{II} = \frac{1}{2} \sum_{i \neq j} \frac{Z_i Z_j}{|\vec{R}_i - \vec{R}_j|}, \tag{3.37}$$

where $\vec{R}_i$ is the position and Z_i is the charge of core i.

3.1.3 PBE functionals

One possible way to model the exchange-correlation effects is to use the Perdew-Burke-Ernzerhof (PBE) functional [47]. We start by writing:

$$E_{xc} = E_x + E_c, \tag{3.38}$$

that is to say that the exchange-correlation energy is divided into exchange and correlation terms. Second thing that needs to be remembered is the local spin density (LSD) approximation:

$$E_{xc}^{LSD} = \int n\epsilon_{xc}^{unif} dr. \tag{3.39}$$

For the correlation term E_c in the GGA we write:

$$E_c^{GGA}[n_\uparrow, n_\downarrow] = \int n[\epsilon_{xc}^{unif}(r_s, \xi) + H(r_s, \xi, t)]dr, \tag{3.40}$$

where r_s is the local Seitz radius:

$$r_s = (\frac{3}{4\pi n})^{\frac{1}{3}}, \tag{3.41}$$

ξ is the relative spin polarization:

$$\xi = \frac{n_\uparrow - n_\downarrow}{n}, \tag{3.42}$$

$n_\uparrow, n_\downarrow$ are the densities for spins up and down, t is a dimensionless density gradient:

$$t = \frac{|\nabla n|}{2\phi k_s n}, \tag{3.43}$$

where ϕ is a spin-scaling factor:

$$\phi(\xi) = \frac{[(1+\xi)^{\frac{2}{3}} + (1-\xi)^{\frac{2}{3}}]}{2}, \tag{3.44}$$

and k_s is the Thomas-Fermi screening wave number:

$$k_s = \sqrt{\frac{4k_F}{\pi a_0}}. \tag{3.45}$$

The first term in 3.40 depends only on density, the second term depends both on the density and the density gradient. We want the term depending

on the gradient to satisfy three conditions. The first condition is that, at the almost uniform case $(t \to 0)$:

$$H \to (\frac{e^2}{a_0})\beta\phi^3 t^2, \tag{3.46}$$

where β is a constant. The second condition we want to be satisfied is that the correlations wanish at the rapidly varying limit $(t \to \infty)$:

$$H \to -\epsilon_c^{unif}. \tag{3.47}$$

The third condition we want is that under high-density limit:

$$H \to (\frac{e^2}{a_0})\gamma\phi^3 ln(t^2), \tag{3.48}$$

where γ is a constant.

These conditions are met by functions:

$$H = (\frac{e^2}{a_0})\gamma\phi^3 ln(1 + \frac{\beta t^2}{\gamma}[\frac{1 + At^2}{1 + At^2 + A^2 + t^4}]), \tag{3.49}$$

where

$$A = \frac{\beta}{\gamma}[e^{-\frac{a_0\epsilon_c^{unif}}{\gamma\phi^3 e^2}} - 1]^{-1}. \tag{3.50}$$

A second dimensionless density gradient s is defined as:

$$s = \sqrt{\frac{r_s}{a_0}}\phi t/c, \tag{3.51}$$

where c is a constant.

We want the exchange energy to satisfy four more conditions. We must have:

$$E_x^{GGA} = \int n e_x^{unif} F_x(s) dr, \tag{3.52}$$

where

$$F_x(0) = 1 \tag{3.53}$$

and

$$e_x^{unif} = -\frac{3e^2 k_F}{4\pi}. \tag{3.54}$$

We also want the exchange energy to satisfy:

$$E_x[n_\uparrow, n_\downarrow] = \frac{E_x[2n_\uparrow] + E_x[2n_\downarrow]}{2}. \tag{3.55}$$

Third additional condition we have is that as $s \to 0$:

$$F_x(s) \to 1 + \mu s^2. \tag{3.56}$$

The fourth additional condition we have is the Lieb-Oxford bound:

$$E_x[n_\uparrow, n_\downarrow] \geq E_{xc}[n_\uparrow, n_\downarrow] \geq -C \int n^{\frac{4}{3}} dr, \tag{3.57}$$

where C is a universal constant.

A simple suitable $F_x(s)$ is:

$$F_x(s) = 1 + \kappa - \frac{\kappa}{1 + \frac{\mu s^2}{\kappa}}, \tag{3.58}$$

where κ is a constant.

3.1.4   GTH pseudopotentials

GTH pseudopotentials are named after Goedecker, Teter and Hutter [48]. In this method the potential V is divided to a local part V_{local}^{PP} and a non-local part $V_{non-local}^{PP}$ [48–50]. The local part is:

$$V_{local}^{PP} = -\frac{Z_{eff}}{r} erf(\alpha^{PP} r) + \sum_{i=1}^{4} C_i^{PP} (\sqrt{2}\alpha^{PP} r)^{2i-2} e^{-(\alpha^{PP} r)^2}, \tag{3.59}$$

where:

$$\alpha^{PP} = \frac{1}{\sqrt{2} r_{loc}^{PP}} \tag{3.60}$$

sets the scale of locality.

The non-local potential is of the form:

$$V_{non-local}^{PP}(r, r') = \sum_{lm} \sum_{ij} \langle r \, | \, p_i^{lm} \rangle h_{ij}^l \langle p_j^{lm} \, | \, r' \rangle, \tag{3.61}$$

where:

$$\langle r \, | \, p_i^{lm} \rangle = N_i^l Y^{lm}(\hat{r}) r^{l+2i-2} e^{-\frac{1}{2}(\frac{r}{r_l})^2}, \tag{3.62}$$

where N_i^l are normalization constants, $Y^{lm}(\hat{r})$ are the spherical harmonics. Because of the Gaussian factors in both the local and the non-local potentials there is a reasonable convergence in both the real space and in the Fourier space.

The free parameters in the pseudopotentials need to be optimized with respect to the functional used. In practice there are many tables of pseudopotentials optimized for different functionals.

3.2 Nudged Elastic Band method

The nudged elastic band method (NEB) is a method for finding a minimum energy path (MEP) between two states [51]. More specifically it finds a minimum energy path between two stable states. That is to say, both the initial and final state need to be local minima of the system energy function.

The nudged elastic band is a chain-of-states method. A reaction pathway is described by a group of images connected with a spring. A nudged elastic band calculation usually starts with a set of states linearly interpolated between the initial and the final state. A schematic is in figure 3.2 [52]. The images are then moved according to the following rules.
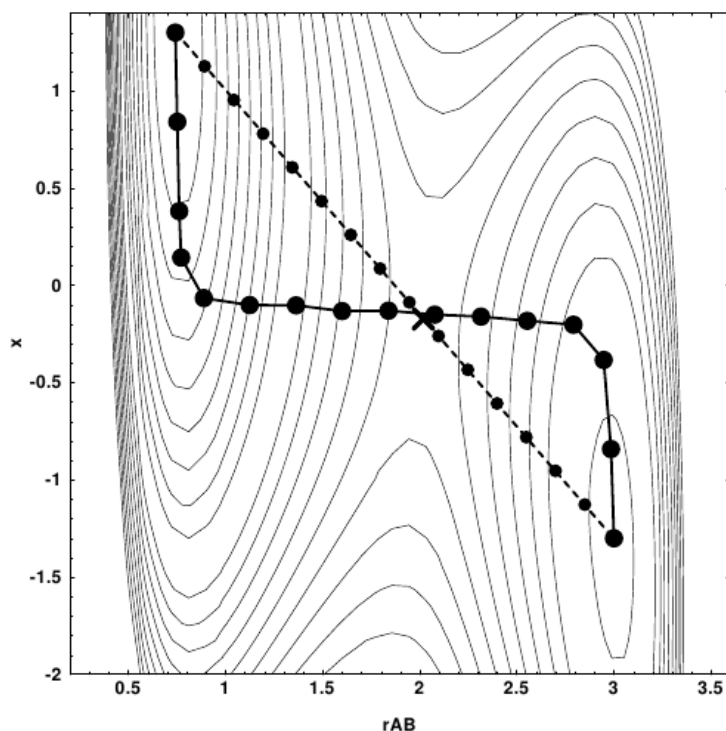
Figure 3.2: A schematic of the Nudged Elastic Band method. Dashed line is the initial chain of of states, and the solid line is the converged one.

A force acting on an images i consists of two components:

$$\vec{F}_i^{NEB} = \vec{F}_i + \vec{F}_i^{spring}, \tag{3.63}$$

where $\vec{F}_i$ is a component due to the potential of the system:

$$\vec{F}_i = -\nabla(R_i) + \nabla(R_i) \cdot \hat{\tau}_i \hat{\tau}_i \tag{3.64}$$

where $\hat{\tau}_i$ is the unit vector towards the higher energy neighbouring image, and the $\vec{F}_i^{spring}$:

$$\vec{F}_i^{spring} = k(|R_{i+1} - R_i| - |R_i - R_{i-1}|)\hat{\tau}_i, \tag{3.65}$$

where the k is the spring constant and the R_i is the position of the image i.

An important variation of the nudged elastic band method is the climbing-image nudged elastic band method (CI-NEB). It proceeds just like the regular nudged elastic band, until a highest energy image l is found. The force acting on l is now defined to be:

$$\vec{F}_l^{CI} = \vec{F}_l - 2\vec{F}_l \cdot \hat{\tau}_i \hat{\tau}_i. \tag{3.66}$$

This means the highest energy image feels no spring force and that it climbs among the highest energy route.

3.3 Bader charge

There are many different ways to define partial charge. One intuitive way to is to divide the space into volumes and define the partial charges as integrals of the charge density over the volumes defined. The division of space into subspaces is done with the so called zero flux surfaces $S(r)$, for which the condition [53, 54]:

$$\nabla n(r) \cdot \hat{u}(r) = 0, \tag{3.67}$$

where $\hat{u}(r)$ is the normal unit vector of $S(r)$ at r, holds.

This definition allows the partition of a molecule into atoms based on the observable charge density $n(r)$.

Bader charge of an atom can now be obtained by integrating the charge density:

$$q_{Bader} = \int_{V_{atom}} n(r)dV, \tag{3.68}$$

where V_{atom} is the volume described by the surface $S(r)$.

3.4 Self-organizing maps

A self-organizing map is an artificial neural network, that is trained with methods of unsupervised machine learning. Every neuron of the network has a weight vector in the same space as the data vectors [55–57].

Assume the input vectors are of dimension n. Now, for every node i there is a weight vector $\vec{w}_i$:

$$\vec{w}_i = [w_{i1}...w_{in}]^T. \tag{3.69}$$

It is now possible to define the winning neuron $q(\vec{x})$ corresponding to an input vector $\vec{x}$:

$$q(\vec{x}) = argmin_i d(\vec{w}_i - \vec{x}), \tag{3.70}$$

where d is the distance function and $argmin$ is the argument of the minimum:

$$argmin_i(f(i)) = \{i | \forall j f(j) \geq f(i)\}. \tag{3.71}$$

Euclidean distance is often used as the distance function.

The update rule for weight vectors is:

$$\vec{w}_i(k + 1) = \vec{w}_i(k) + n_{qi}(k)[\vec{x}(k) - \vec{w}_i(k)], \tag{3.72}$$

where k is the iteration number and n_{qi} is the neighbourhood function of the winning neuron q. There are several common ways to define the neughbourhood function. One way to define it is to have a predefined neighbourhood

$N_q(k)$ and have the neighbourhood function be constant for all the neurons in there:

$$n_{qi}(k) = \mu(k), \tag{3.73}$$

where $\mu(k)$ is the learning parameter that decreases with iteration number k according to some predetermined strategy. The learning parameter needs to satisfy the condition:

$$0 < \mu(k) < 1. \tag{3.74}$$

When training a self-organizing map, there are two phases, ordering phase and convergence phase. Initially the learning parameter is close to one, and the updates are large. This way the ordering of weight vectors is carried out. Then the learning parameter is decreased to make the training more stable. In the convergence phase the learning parameter is decreased still and the map is fine tuned.

Important term related to self-organizing maps is the component plane. When the values of a selected component of the weight vectors are represented on the self-organizing map grid, it is called a component plane.

Another important tool related to self-organizing maps is the unified distance matrix, also called the U-matrix. The U-matrix contains the distances between adjacent weight vectors in the map. It also contains the average value of the distance of a neuron from its neighbours.

When using two-dimensional maps it is common to visualize component planes and U-matrices using a colored grid. Looking at the distances between weight vectors as seen on the U-matrix visualization can give information about the distribution of the input data.

Chapter 4

Geometries

This chapter introduces the geometries of the fullerenes discussed in this thesis. The first fullerene introduced is the pristine C_{60}. After that $C_{59}N$ is discussed. Then C_{180} and $C_{179}N$ are introduced. Besides the bond lengths of the fullerenes, this chapter also introduces the naming conventions for different sites at the fullerenes.

4.1 Geometry of C_{60}
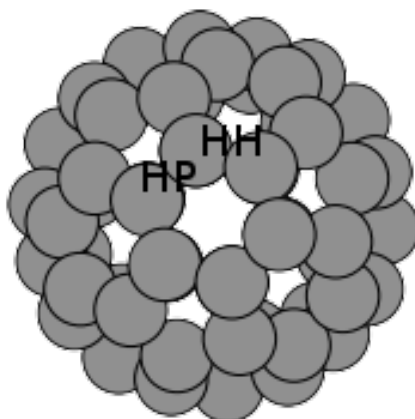
Figure 4.1: Geometry of the pristine C_{60} fullerene and the names of the sites on it. HP stands for hexagon-pentagon and HH stands for hexagon-hexagon.

In this thesis C_{60} means an icosahedral fullerene defined with indices $(1, 1)$. It consists of 60 carbon atoms positioned in a spherical cage. The cage consists of pentagons and hexagons. There are twelve pentagons.

The geometry of the C_{60} is in figure 4.1. In the pristine fullerene there are essentially two kinds of C-C bonds. First one is corresponds to a connection between a hexagon and a pentagon, the second one corresponds to a connection between a hexagon and a hexagon. Hexagon-pentagon site is marked with HP and hexagon-hexagon is marked with HH. Pentagons on the fullerene could also be called five-membered rings and the hexagons could be called six-membered rings.

Every side of a pentagon is connected to a side of a hexagon. In a hexagon, three sides are connected to pentagons and three sides to other hexagons. This means that there are five HP sites in a pentagon, and in a hexagon there are three HP sites and three HH sites.

Table 4.1: Calculated bond lengths of C_{60} in Å. Calculations were done at the PBE/TZVP level of theory. The net charge q of the system is given in e.

site	q=0	q=-1	q=-2	q=-3
HP	1.45	1.45	1.44-1.46	1.44-1.46
HH	1.40	1.40-1.41	1.40-1.42	1.40-1.42

Table 4.1 shows the calculated bond lengths of the C_{60}. We can see that the accuracy of the calculated bond lengths is of the order of 1 pm. Ideally the bond lengths at similar places should be the same. In practice there is some asymmetry in the optimized structure.

4.2   Geometry of C$_{59}$N
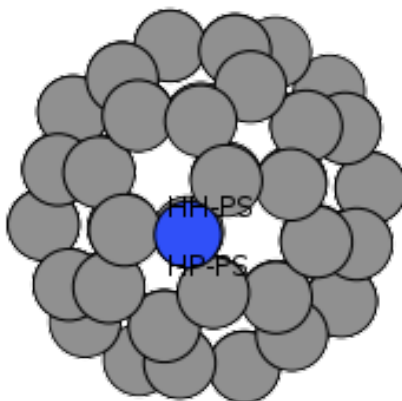
Figure 4.2: Geometry of the C$_{59}$N fullerene. There are now two different kinds of HP and HH sites. The HP sites next to the nitrogen atom are called HP-Pauling. The HH site next to the nitrogen atom is called HH-Pauling.

C$_{59}$N is a C$_{60}$ fullerene, where one of the carbon atoms has been substituted with a nitrogen atom. In C$_{60}$ all carbon atoms are equivalent, so it does not make a difference where the nitrogen substituted site is located. The nitrogen atom gives a natural way to name the sites on the fullerene. In the pristine fullerene there are two different kinds of sites, HH and HP. The doped fullerene has several different kinds of HH and HP sites. Sites where the nitrogen atom are involved are called HH-Pauling and HP-Pauling. These are HH and HP sites, where one of the involved atoms is a nitrogen atom and the other is a carbon atom. Sites where all the atoms involved are carbon atoms are called HH-CC and HP-CC. HH-Pauling site and HP-Pauling site are shown in figure 4.2.

Table 4.2 shows the effect of charge on the bond lengths near the nitrogen atom. We can see that the changes in the bond lengths due to the charge are of the order of 1 pm. This behaviour is similar to the pristine fullerene. When there is net charge in the system, the bond lengths of HP-PS and HH-PS are about the same.

A thing that should be remembered is that the nitrogen atom brings an unpaired electron to the system. This means that there is some spin density spread out to the system. Figure 4.3 shows an isosurface of this density. We

Table 4.2: Calculated bond lengths of $C_{59}N$ near the nitrogen atom in Å. Calculations were done at the PBE/TZVP level of theory. The net charge q of the system is given in e.

site	q=0	q=-1	q=-2	q=-3
HP-PS	1.43	1.42	1.43	1.43
HH-PS	1.40	1.43	1.43	1.42
HP-CC	1.44	1.44	1.43	1.43
HH-CC	1.39	1.41	1.42	1.42

see that a large amount of it goes to the nitrogen, but we also see that the atom with most magnetic moment is the carbon atom next to the nitrogen in the HH-PS site. The magnetic moment of the carbon atom next to the nitrogen atom having the largest amount of magnetic moment is 0.17 μ_B, other atoms have less.

It is important to keep in mind that different directions on the fullerene are no longer the same when there is nitrogen doping. This should be kept in mind when thinking about what is far and what is near the nitrogen atom.
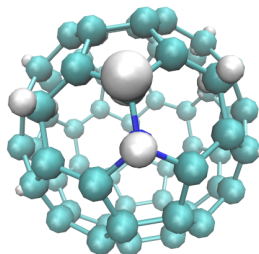
Figure 4.3: Isosurface of the spin density on the $C_{59}N$ fullerene. Calculations were done at the PBE/TZVP level.

4.3 Geometry of C_{180}

In this thesis C_{180} means an icosahedral fullerene defined with indices $(3, 0)$. It obeys the isolated pentagon rule. There are essentially three different kinds of polygons on the C_{180}, pentagons, and two different kinds of hexagons. Every pentagon is surrounded by five hexagons. First kind of hexagon is touching one pentagon and five hexagons. The second kind of hexagon is surrounded by six hexagons.

Figure 4.4 shows the geometry of the C_{180} fullerene and the naming convention for different sites. As was the case with C_{60}, HP is the hexagon-pentagon connection. In C_{180} there are three different hexagon-hexagon connections. HH1 is the site of a hexagon-hexagon connection, where both hexagons are touching a pentagon. HH2 is a site, where one of the hexagons is touching a pentagon and the other is touching only hexagons. HH3 is a site that is exactly in the halfway from one pentagon to another.
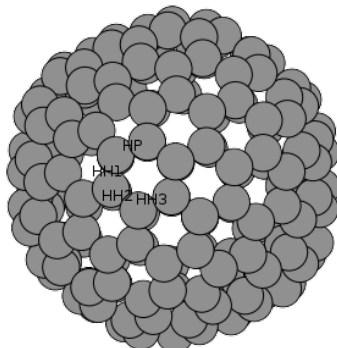
Figure 4.4: Geometry of the C_{180} fullerene. HP stands for hexagon-pentagon, HH1, HH2, and HH3 stand for different hexagon-hexagon sites.

Table 4.3: Calculated bond lengths of C_{180} in Å. Calculations were done at the PBE/TZVP level. The net charge q of the system is given in e.

site	q=0	q=-6	q=-12
HP	1.43	1.43	1.43
HH1	1.39	1.41	1.42
HH2	1.45	1.44	1.43
HH3	1.45	1.47	1.49

Table 4.3 shows the effect of charge on the bond lengths of the C_{180} fullerene. We see that the geometry of the pentagons does not change much with extra charge, but different HH bonds are affected. Adding charge increases the bond lengths by order of picometers along hexagons that are touching pentagons. We also see that the bond lengths decrease by the order of picometers with charge when the site considered involves a hexagon touching only other hexagons. We can also see that the changes in the bond lengths are of the order of several picometers.

4.4 Geometry of $C_{179}N$

$C_{179}N$ is a C_{180} fullerene, where one of the carbon atoms has been substituted with a nitrogen atom. In C_{180} all the carbon atoms are not equivalent, so it is important to consider, where the substitution happens and what is energetically the most favourable option.

Table 4.4: Relative total energy E_{rel} in eV of different $C_{179}N$ fullerenes

Location of nitrogen	E_{rel}
pentagon	0
hexagon next to a pentagon	0.39
hexagon next to hexagons	0.50

Table 4.4 shows the relative energies of several possible nitrogen substitution sites. The most favourable nitrogen substitution site is at a pentagon. The naming convention for sites on $C_{179}N$ follows the convention for C_{180} and $C_{59}N$.

Similarly to $C_{59}N$, also $C_{179}N$ has distribution for the spin density. This means that it is important to consider the directions when talking about what is far and what is near the nitrogen atom. An isosurface of the spin density can be seen in figure 4.5.
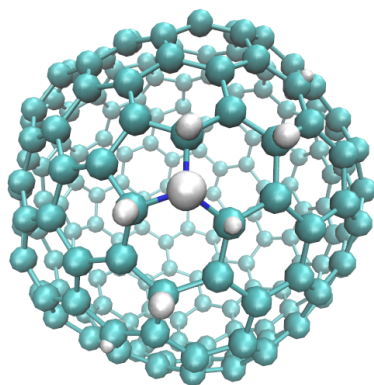
Figure 4.5: Spin density isosurface on the $C_{179}N$ fullerene. Calculations were done at the PBE/TZVP level of theory.

Chapter 5

Adsorption

In this chapter the adsorption of oxygen to the fullerenes is discussed. The adsorption energy E_{ads} is calculated as:

$$E_{ads} = E_{fullerene+O_2} - (E_{fullerene} + E_{O_2}), \qquad (5.1)$$

that is to say the energy of the system after the adsorption minus the sum of energies of the original molecules.

Adsorption can be divided to chemisorption and physisorption. In this thesis the adsorption studied is chemisorption.

5.1   Adsorption on C_{60}

There are two topologically different possible adsorption sites on the pristine C_{60} fullerene. The first one is at the HP site and the second one is at the HH site.

Figure 5.1 shows the oxygen molecule on the HP adsorption site of C_{60}. The naming convention for the oxygen atoms is that the atom with the larger Bader charge is called O(1), and the oxygen atom with smaller Bader charge is called O(2). The carbon atoms corresponding to these oxygen atoms are called C(1) and C(2). This naming convention is followed in all the adsorption cases in this thesis.
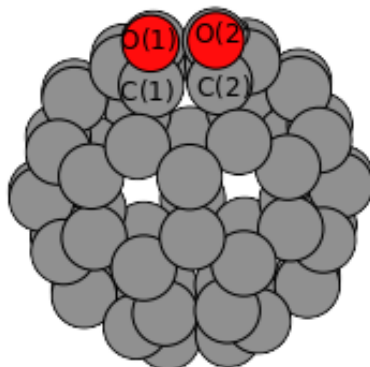
Figure 5.1: Oxygen molecule on the HP adsorption site. O(1) is the oxygen atom with larger Bader charge, O(2) is the one with smaller Bader charge. C(1) is the carbon atom corresponding to O(1), and C(2) corresponds to O(2).

Table 5.1: Total charges in e, bond lengths in Å, and adsorption energies in eV on the charged C_{60}. Calculations were done at the PBE/TZVP level of theory.

Site	charge	d_{C-O}	d_{O-O}	d_{C-C}	E_{ads}
HP	0	1.47	1.52	1.59	0.36
	-1	1.48	1.53	1.59	-0.24
	-3	1.51	1.53	1.58	-0.99
HH	0	1.46	1.51	1.57	-0.35
	-1	1.47	1.51	1.57	-0.50
	-3	1.49	1.52	1.57	-0.81

Table 5.1 shows the bond lengths and adsorption energies for the adsorptions on the C_{60}. We can see that the carbon-carbon and oxygen-oxygen bond lengths are relatively independent of the charge of the system. The carbon-oxygen bond lengths however change several picometers with charge. We also see that adding charge to the fullerene makes the adsorption event more and more favourable energetically.

At both HH and HP the oxygen molecule forms a quadrilateral structure

Table 5.2: Bader charges in e for the oxygen atoms O(1) and O(2) and the carbon atoms C(1) and C(2) binding to them.

Site	charge	O(1)	O(2)	C(1)	C(2)
HP	0	-0.45	-0.45	0.42	0.41
	-1	-0.47	-0.48	0.38	0.41
	-3	-0.51	-0.52	0.31	0.39
HH	0	-0.45	-0.46	0.41	0.45
	-1	-0.47	-0.48	0.40	0.43
	-3	-0.50	-0.51	0.36	0.41

with the carbon atoms. O(1) is the oxygen with the smaller Bader charge and O(2) is the oxygen with larger Bader charge. O(1) is located at the top of carbon atom C(1) and O(2) is on top of C(2). The quadrilateral structure is then formed by atoms O(1), O(2), C(1), and C(2). Table 5.2 shows the Bader charges for these atoms. We can see that the charges are of opposite sign and that the absolute values of the partial charges are about the same. The unit formed by a carbon atom and the oxygen atom on top of it is therefore essentially neutral. This is a strongly polarized bond. When charge is added to the fullerene, we see that the Bader charges change. The changes in Bader charges roughly correspond to the extra charge being divided evenly among all the atoms on the molecule.

5.2 Adsorption on $C_{59}N$

There are many more topologically different adsorption sites on $C_{59}N$ than there are on C_{60}. We are interested in the effects caused by the nitrogen atom.

Table 5.3: Adsorption energies in eV for different adsorption sites of $C_{59}N$. Calculations were done at the PBE/TZVP level of theory.

Adsorption site	E_{ads}	E_{ads} in C_{60}
HP-Pauling	-0.15	
HP-CC, pentagon doped	-0.17	
HP-CC, hexagon doped	-0.61	
HP-CC, doping several polygons away	0.33	0.36
HP-CC, doping several polygons away, oxygen atoms next to carbons with magnetic moment	0.18	
HH-Pauling	-0.71	
HH-CC, hexagon doped	-0.52	
HH-CC, doping several polygons away	-0.37	-0.35

Table 5.3 shows the adsorption energies for different sites of the neutral $C_{59}N$. First thing we see that the HP-CC and HH-CC sites far away from the nitrogen site have the same adsorption energies as the HP and HH sites of the pristine C_{60}. Second thing that is noticed is that the magnetic moment that is localized on the carbons relatively far from nitrogen have an effect on the adsorption energy.

Energetically the most favourable adsorption site is the HH-Pauling, followed by HP-CC and HH-CC near a hexagon with a nitrogen atom. We also see that most of the sites have a negative adsorption energy, which means that the adsorption is energetically favourable compared to the oxygen molecule being free.

Table 5.4 shows the effect charge has on the adsorption energies at the adsorption sites near the nitrogen atom. We can see that adding electrons to the fullerene system makes the oxygen molecules to bind more strongly with the fullerene. There is a clear trend of adsorption becoming more and more favourable with extra electrons. However, we also see that the energy at some sites changes more than at others. We see large changes at the energies of the HP-CC sites when the first extra electron is added. There is almost no change in the adsorption energies at the HH-CC and HH-Pauling sites at that point.

Table 5.4: Adsorption energies in eV at different sites of $C_{59}N$ fullerene with different total charges in e. Calculations were done at the PBE/TZVP level of theory.

Adsorption site	Charge	E_{ads} (eV)
HP-CC, nitrogen in pentagon	0	-0.17
	-1	-0.58
	-2	-0.83
	-3	-1.09
HP-CC, nitrogen in hexagon	0	-0.61
	-1	-1.14
	-2	-1.26
	-3	-1.40
HH-CC	0	-0.52
	-1	-0.59
	-2	-0.72
	-3	-0.88
HH-Pauling	0	-0.71
	-1	-0.68
	-2	-0.96
	-3	-1.19

5.3 Adsorption on C_{180}

The structure of the C_{180} is a bit more complicated than that of C_{60}. In C_{60} every carbon atom is topologically similar to the other carbon atoms. In the C_{180} fullerene there are several topologically different carbon atoms. Similarly to the two possible adsorption sites of the C_{60}, there are four possible adsorption sites for the oxygen molecule on the C_{180}.

Table 5.5 shows the structural properties and adsorption energies for oxygen adsorption on C_{180} fullerene. We see that for the neutral fullerene all the adsorption energies are positive, which means that it is favourable for the oxygen molecule to stay free. When charge is added the adsorption energies decrease. Adsorption at the HP site is energetically favourable when the charge of the fullerene is -6. Adsorption at sites HH1 and HH2 is at charge of -6 still energetically unfavourable. At charge -6 the oxygen can undergo a dissociative adsorption at the HH3 site.

At charge -12 all adsorption sites except HH2 lead to dissociative adsorption. At HH2 the oxygen molecule stays intact and points upwards from the

Table 5.5: Adsorption energies in eV and bond lengths in Å at different sites of C_{180} fullerene with different charges in e. Calculations were done at the PBE/TZVP level of theory.

Site	charge	d_{C-O}	d_{C-O}	d_{O-O}	d_{C-C}	E_{ads}
HP	0	1.48	1.48	1.52	1.55	0.54
	-6	1.51	1.51	1.53	1.55	-0.33
*	-12	1.38	1.38	2.87	1.67	-2.67
HH1	0	1.46	1.46	1.51	1.53	0.56
	-6	1.48	1.53	1.52	1.54	0.42
*	-12	1.39	1.41	2.76	1.60	-1.61
HH2	0	1.49	1.47	1.52	1.60	1.13
	-6	1.54	1.50	1.51	1.59	0.21
	-12	2.84	1.55	1.45	1.53	-1.06
HH3	0	1.47	1.47	1.50	1.68	0.36
*	-6	1.23	1.24	2.64	3.03	-2.38
*	-12	1.26	1.26	2.53	3.02	-3.44

* dissociative adsorption.

surface of the fullerene.

The dissociative adsorption at the HH3 site also creates a hole to the fullerene. Besides the oxygen-oxygen bond breaking also the carbon-carbon bond at the HH3 site breaks. The carbon atoms bonded with the oxygen atoms rise upwards from the surface of the fullerene.

Table 5.6: Bader charges in e for the oxygen atoms O(1) and O(2) and the carbon atoms C(1) and C(2) near them on neutral C_{180}.

Site	O(1)	O(2)	C(1)	C(2)
HP	-0.42	-0.44	0.36	0.43
HH1	-0.41	-0.45	0.36	0.44
HH2	-0.43	-0.45	0.34	0.33
HH3	-0.46	-0.47	0.42	0.50

Bader charges for atoms O(1), O(2), C(1), and C(2) on neutral C_{180} are in table 5.6. We can see that the oxygen atoms have a negative Bader charge, and the corresponding carbon atoms have a positive Bader charge of the same magnitude. This is similar to what happens with C_{60}, see table 5.2.

5.4 Adsorption on $C_{179}N$

In the case of pristine C_{180} fullerene there are only a few topologically different adsorption sites. In the case of doped fullerenes there are lot less symmetries, so there are many more different adsorption sites. However, as we saw in the case of the 60 atom fullerene, when we are far away from the doped site, the doped fullerene acts like the undoped one. This allows us to only look at the cases in the immediate neighbourhood of the doped site.

Table 5.7: Adsorption energies in eV of the oxygen adsorption on the $C_{179}N$ with different total charges in e. Calculations were done at the PBE/TZVP level of theory.

Site	charge	E_{ads}
HP	0	0.05
	-6	-0.64
*	-12	-2.64
HH1	0	0.43
*	-6	-1.35
**	-12	
HH2a	0	0.26
	-6	-0.39
*	-12	-2.24
HH2b	0	0.69
	-6	-0.10
**	-12	
HH3	0	0.44
	-6	0.26
*	-12	-3.91

* dissociative adsorption. ** no adsorption.

Table 5.7 shows the adsorption energies for different adsorption sites on the $C_{179}N$. In general, adding the nitrogen atom in the fullerene makes the adsorption event more favourable energetically. The only site where this does not hold is the HH3 site where the adsorption energy goes up by 0.08 eV when comparing the doped and undoped fullerenes.

Adding charge to the system makes the adsorption more favourable energetically. The adsorption energies go down for all the sites near the nitrogen atom. We again see that when the charge is large enough, the adsorption happens dissociatively.

We see that there is a difference in adsorption energies for the variations of the HH2 adsorption sites. This means that it is energetically favourable for the oxygen molecule to be bind to the carbon atom next to the nitrogen atom.

Chapter 6

Oxygen dissociation

There are many different ways an oxygen molecule can dissociate on a fullerene as elucidated below. There are also many different sites the oxygen molecule may be be adsorbed to the fullerene as discussed previously. Every adsorption site is related to several different dissociation pathways.

A relevant quantity related to dissociation is the dissociation energy E_{dis}. It is defined as:

$$E_{dis} = E_{fullerene+O+O} - (E_{fullerene} + E_{O_2}), \qquad (6.1)$$

that is to say, the total energy of the system after the dissociation minus the sum of the energies of the original molecules.

Dissociations, where the oxygen atoms end up to the same side of the adsorption site are called symmetric dissociations. When this is not the case, the dissociation is asymmetric.

6.1 Dissociation on C$_{60}$

As previously discussed, there are two different adsorption sites on a pristine C$_{60}$ fullerene. There are several possible dissociation pathways from both of the adsorption sites. The oxygen molecule may dissociate symmetrically or asymmetrically. In the symmetric dissociation the oxygen atoms end up in the same polygon. In the asymmetrical dissociation this is not the case.

Table 6.1 shows the dissociation energies for several oxygen dissociations on the pristine C$_{60}$ fullerene. We see as a general trend that the dissociation energies tend to increase with charge. The only dissociation pathway that does not follow this trend is the HP-sym 1 case. In that case the oxygen atoms move from the HP site to the pentagon. At the pentagon they locate themselves on two sides of the pentagons and also break the carbon-carbon

Table 6.1: Dissociation energies in eV on pristine C_{60} for different total charges in e. Calculations were done with at the PBE/TZVP level of theory.

Adsorption site	Dissociation	charge	E_{dis}
HP	sym 1	0	-2.28
		-1	-2.42
		-2	-1.28
		-3	-1.58
	sym 2	0	-1.85
		-1	-1.99
		-2	-2.14
		-3	-2.18
	asym 1	0	-1.38
		-1	-1.46
		-2	-1.55
		-3	-1.59
HH	sym 1	0	-1.05
		-1	-1.25
		-2	-1.46
		-3	-1.61
	asym 1	0	-0.24
		-1	-0.96
		-2	-1.65
		-3	-1.76

bonds there. When there is a lot of charge in the fullerene, the oxygen-carbon bonds elongate, and the carbon-carbon bonds stay intact.

At the dissociation configurations the oxygen atoms tend to form epoxy structures with the carbon atoms. A second possibility besides the triangular structure is a chain-like formation where an oxygen atom is bonded with two carbon atoms, but the carbon atoms are not bonded with each other. The triangular configurations are more common than the chain-like ones, and when charge is added to the system the chain-like configurations have the tendency to turn into triangular ones.

Figure 6.1 shows the energy profile of the dissociation in the case HP-sym 2 for different total charges. The oxygen molecule is first adsorbed to the HP site, and then it dissociates in a way that both the oxygen atoms end up in the sides of the hexagon of HP site. Adding charge to the system makes the adsorption energetically more favourable. Also the dissociation is
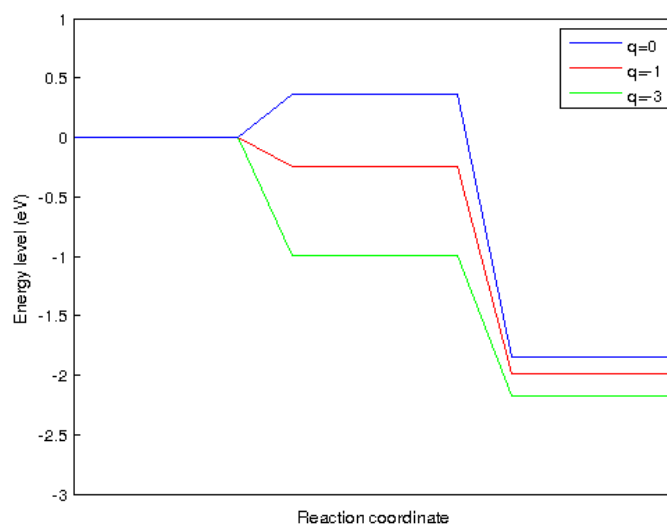
Figure 6.1: An example of a reaction energy diagram for oxygen dissociation on C_{60}. This is the HP-sym 2 dissociation case. Energy of zero corresponds to the free oxygen molecule, and the plateaus correspond to the adsorption configuration and dissociation configuration.

more favourable when more charge is added, but that the change is smaller. The change in adsorption energy per electron is of the order 0.3 eV, and the change in dissociation energy per electron is of the order 0.1 eV. The change in the adsorption energy is therefore about three times as large as the change in the dissociation energy. Other dissociation pathways besides the HP-sym 2 show similar behaviour.

The adsorbed configuration and the dissociated configuration are both local minima of the energy. There is also an energy barrier between them. Figure 6.2 shows the energy profiles of the HP-sym 2 dissociation. It should be noticed that figures 6.1 and 6.2 have different energy scales. Energy barrier for the oxygen dissociation on the neutral fullerene is 0.58 eV, fullerene with charge -1 has barrier of 0.45 eV, and fullerene of charge -3 has barrier of 0.12 eV. We can therefore see that adding charge to the system decreases the energy barrier for dissociation.
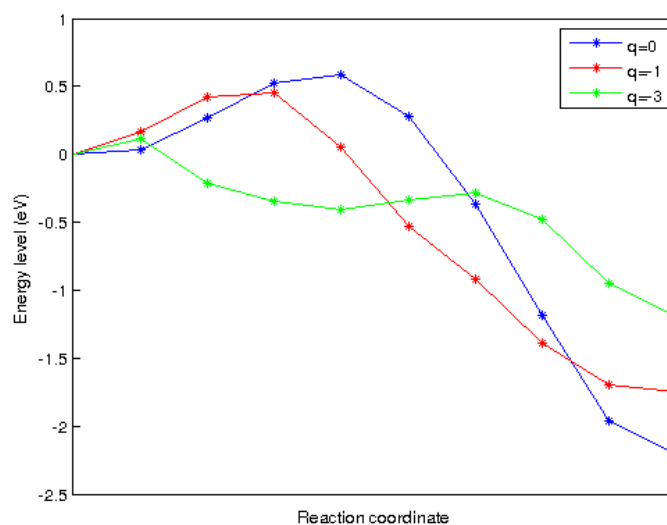
Figure 6.2:   Charge effects on the minimum energy path of the HP-sym 2 dissociation, as given by the Nudged Elastic Band method. Energy level zero corresponds to the energy of the adsorption configuration.

6.2   Dissociation on $C_{59}N$

There are many more different adsorption sites on $C_{59}N$ than there are on C_{60}. There are again several different dissociation pathways relating to each of these adsorption sites.

Table 6.2 shows some dissociation energies on $C_{59}N$. One thing we see is that when the oxygen atoms move symmetrically away from the nitrogen we obtain the same dissociation energies as we did on the symmetrical dissociations on the pristine fullerene. This tells us what exactly is 'far' from the substitution site.

Dissociation configurations where the oxygen atoms are closer to the nitrogen atom tend to be lower in energy than the ones where the oxygen atoms are far away from the nitrogen atom.

Adding charge to the system does not affect the energy of all the dissociation configurations the same way. The sites that are far from the nitrogen atom behave just like the sites on pristine fullerene. Some sites show no change in their energy. Some sites show larger changes in energy that correspond to breaking of carbon-carbon bonds.

Table 6.2: Dissociation energies in eV on $C_{59}N$ for different total charges in e. Calculations were done at the PBE/TZVP level of theory.

Adsorption site	Dissociation	charge	E_{dis}
HP-CC, pentagon doped	sym 1	0	-1.86
		-1	-1.92
		-2	-2.01
		-3	-2.12
	sym 2	0	-1.04
		-1	-1.13
		-2	-1.23
		-3	-1.35
	asym 1	0	-1.07
		-1	-1.23
		-2	-1.54
		-3	-1.86
HP-CC, hexagon doped	sym 1	0	-1.64
		-1	-2.62
		-2	-2.87
		-3	-3.15
	sym 2	0	-2.33
		-1	-2.42
		-2	-2.43
		-3	-2.45
	asym 1	0	-1.70
		-1	-2.07
		-2	-2.17
		-3	-3.15
HH-CC	sym 1	0	-1.20
		-1	-1.25
		-2	-1.29
		-3	-1.35
	sym 2	0	-1.94
		-1	-1.88
		-2	-1.88
		-3	-1.90
	asym 1	0	-1.44
		-1	-1.82
		-2	-2.03
		-3	-2.27
	asym 2	0	-1.07
		-1	-1.58
		-2	-1.70
		-3	-1.83

The effects of extra charge seem to be larger on the asymmetrical dissociation configurations. We see that the more charge is added to the system, the more favourable the asymmetric dissociations become.
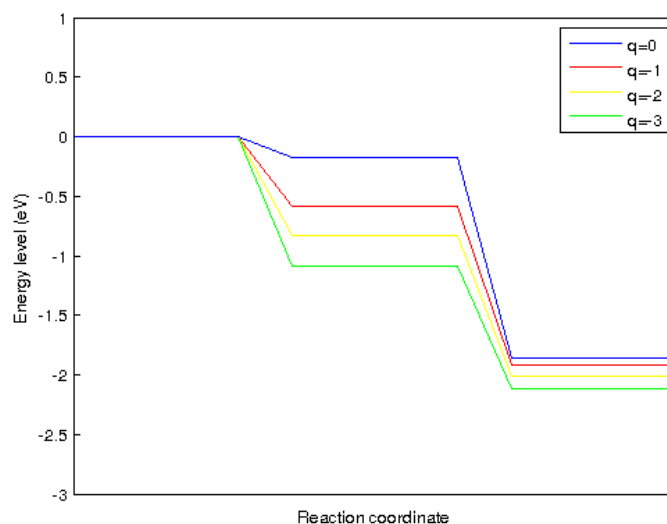

Figure 6.3: An example of a reaction energy diagram for oxygen dissociation on $C_{59}N$. Energy of zero corresponds to the free oxygen molecule, and the plateaus correspond to the adsorption configuration and dissociation configuration.

Figure 6.3 shows an example energy profile of a dissociation on $C_{59}N$. There are similarities to the dissociation on pristine fullerene. Both the adsorption and dissociation get more favourable when charge is added. Also we can see that the change in adsorption energy is larger than the change in dissociation energy. The case in figure 6.3 is similar to the one in figure 6.1, as they both correspond to the oxygen atoms moving from the HP site to the sides of a hexagon.

Figure 6.4 shows the energy profile of the symmetric dissociation of the oxygen molecule symmetrically from the HP site away from the nitrogen atom. The energy barrier for the dissociation is 0.34 eV. Compared to the similar dissociation on the pristine fullerene, as seen in figure 6.2, we see that the barrier is lower than that of the neutral fullerene, and that of the pristine fullerene with charge of -1. However, the barrier for the dissociation on the neutral $C_{59}N$ is higher than the barrier on the pristine fullerene with charge of -3 elementary charges.
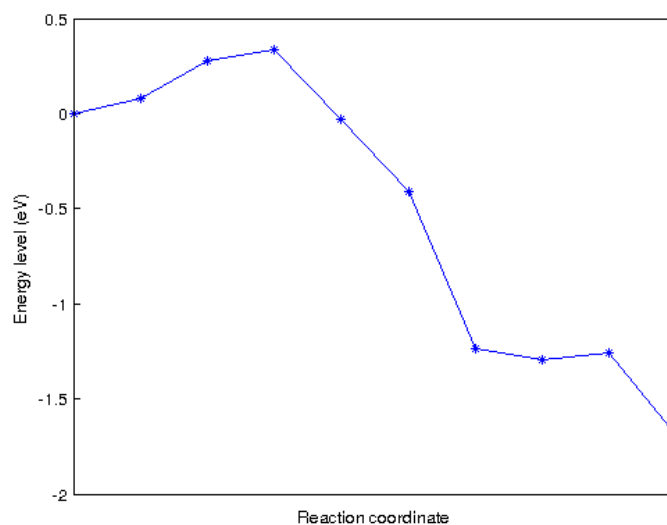
Figure 6.4: An example of the minimum energy path of oxygen dissociation on neutral $C_{59}N$. Compare to figure 6.2.

We can see that even when the energies of the adsorption and dissociation configurations are essentially the same in the case of pristine and the nitrogen-doped fullerene, the energy barriers between the configurations are different.

A second thing that can be seen in figure 6.4 is that there is a plateau in energy near the end of the reaction. The plateau corresponds to situation, where an oxygen atom is on top of a carbon atom next to the nitrogen atom. Depending on the total charge of the system, it is either more favourable for the oxygen atom to be located on top of the carbon atom next to the nitrogen atom, or in a triangular form with two carbon atoms.

6.3 Dissociation on C_{180}

There are four adsorption sites on the pristine C_{180}. Every one of them is associated with several different dissociation pathways.

Table 6.3 shows the dissociation energies for different dissociation pathways. We can see that adding charge to the fullerene makes the dissociation more favourable energetically. We can see that with neutral fullerene the symmetric dissociations are favourable compared to the asymmetric dissociations. However, when charge is added the asymmetric dissociations become more favourable energetically.

Table 6.3: Dissociation energies in eV for the different dissociation configurations on the pristine C_{180} fullerene with different total charges q in e. Calculations were done at the PBE/TZVP level of theory.

Adsorption site	Dissociation	E_{dis}		
		q=0	q=-6	q=-12
HP	sym 1	-0.87	-1.02	-1.25
	sym 2	-0.65	-0.69	-0.95
	asym 1	-0.35	-0.80	-2.44
HH1	sym 1	-0.22	-0.58	-1.16
	asym 1	0.32	-0.78	-1.44
HH2	sym 1	-0.84	-1.30	-2.94
	sym 2	-0.71	-0.83	-1.21
	asym 1	-0.03	-0.75	-2.67
HH3	sym 1	-0.01	-0.41	-1.08
	asym 1	0.64	-0.48	-1.20

We can see that change in dissociation energy per six extra electrons is of the order of 1 eV for the asymmetric dissociations. For the symmetric cases the change is of the order 0.3 eV. The difference in the change is again of the order of three, as was the case in C_{60}.

Figure 6.5 shows an example of the changes in the dissociation energies caused by adding charge to the system. Figure 6.5(a) has figures 6.5(b), 6.5(c), and 6.5(d) combined. This example case shows several ways charge can affect the dissociation energy. First case is shown in figure 6.5(b). In this case charge causes a change of only 0.04 eV, so it can be said that the energy is not affected by the charge. Second case, as seen in figure 6.5(c), shows a change of 0.15 eV in the dissociation energy. Both of these are symmetric dissociations. The third case, as seen in figure 6.5(d) shows the charge effects on an asymmetric configuration. We see that adding six electrons to the systems changes the dissociation energy of the asymmetric dissociation by 0.45 eV.
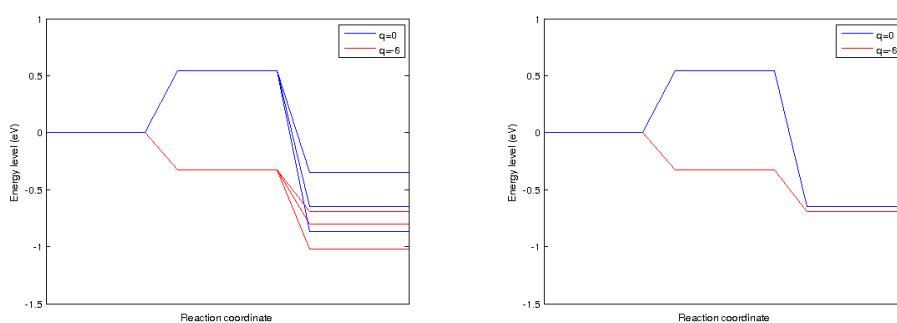
(a) Several dissociation pathways from the HP site.

(b) Symmetric dissociation from the HP site with $\Delta E_{dis} = 0.04$eV.
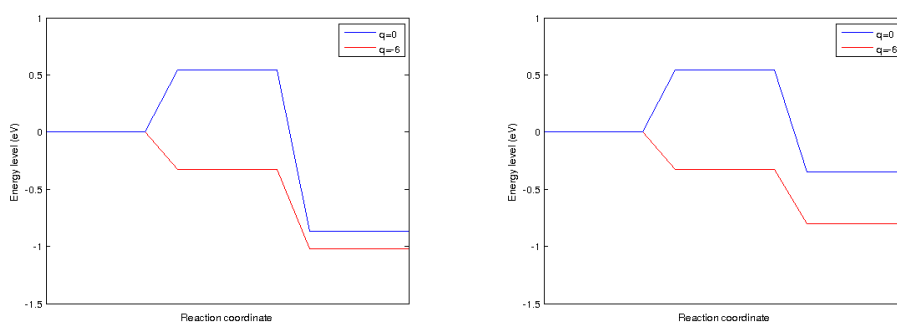
(c) Symmetric dissociation from the HP site with $\Delta E_{dis} = 0.15$eV.

(d) Asymmetric dissociation from the HP site with $\Delta E_{dis} = 0.45$eV.

Figure 6.5: Charge effects on dissociation energies on the pristine C_{180} fullerene. Energy level zero corresponds to the free oxygen molecule configuration.
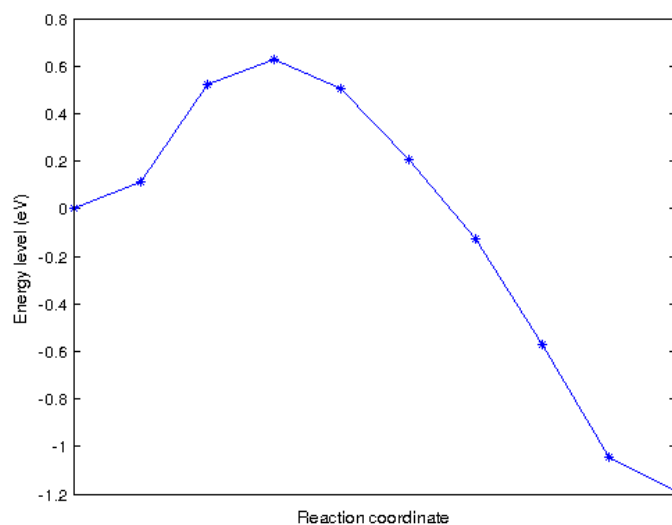
Figure 6.6: An example of the energy profile of oxygen dissociation on neutral C_{180}. Compare to figures 6.2 and 6.4.

Figure 6.6 shows an example of a energy profile of a oxygen dissociation on C_{180}. In this example the dioxygen molecule starts at the HP site and the oxygen atoms end at the sides of the neighbouring hexagon, and forming triangular structures with the carbon atoms. The reaction barrier for this dissociation is 0.63 eV. This value is quite close to the barrier of 0.58 eV seen on neutral C_{60}. Figure 6.6 shows the same dissociation reaction as does the blue line in 6.5(b). It should be kept in mind that these two figures have different scales for the energy. Zero energy in figure 6.5(b) is the sum of total energies of fullerene and oxygen, but zero energy in figure 6.6 is the total energy of the adsorption configuration. This explains the different values in the energies in the figures.

6.4 Dissociation on $C_{179}N$

Fullerene $C_{179}N$ has more adsorption sites than does C_{180}. Far away from the nitrogen atom the sites behave just like the sites on the pristine fullerene. In this case the difference is seen in dissociation from HH3 site. When the oxygen molecule moves away from the nitrogen, the dissociation energy goes exactly like in the case of pristine fullerene, but when the oxygen atoms move towards the nitrogen atom, the energies are different. This gives us an accurate way to say what is near and what is far.

Table 6.4: Dissociation energies in eV for the different dissociation configurations on the $C_{179}N$ fullerene for different total charges q in e. Calculations were done at the PBE/TZVP level of theory.

Adsorption site	Dissociation	E_{dis} (eV)		
		q=0	q=-6	q=-12
HP	sym 1	-0.50	-1.73	-4.21
	sym 2	-0.59	-1.76	-4.21 *
	asym 1	-0.17	-1.73 *	-4.21 *
	asym 2	-0.68	-1.76 *	-4.21 *
HH1	sym 1	-0.45	-1.63	-3.16
	sym 2	-0.35	-0.84	-3.09
	asym 1	-0.40	-1.13	-3.16 *
	asym 2	-0.23	-1.35	-3.09 *
HH2a	sym 1	-0.62	-1.75	-3.15
	sym 2	-0.18	-0.93	-3.28
	asym 1	-0.84	-1.75 *	-3.15 *
HH2b	sym 1	-0.58	-1.16	-4.53
	sym 2	0.05	-0.66	-1.42
	asym 1	-0.42	-0.74	-2.60
	asym 2	-0.28	-0.72	-3.19
HH3	sym 1	-0.42	-0.84	-2.60
	sym 2	-0.01 **	-0.41 **	-1.08 **
	asym 1	0.17	-0.56	-2.37
	asym 2	-0.42	-1.02	-2.60 *

* same final state as earlier. ** Same as the dissociation on the pristine fullerene.

Table 6.4 shows the effect charge has on the dissociation energies. It is interesting to see that when charge is high, there are relatively few different

dissociation configurations. When charge is -12, there are fewer minimum energy configurations than there are on the neutral fullerene. This effect is also seen to a lesser degree in the fullerene of charge -6.

Chapter 7

Comparisons

Previous chapters have shown that there are differences in the adsorption and dissociation energies for different fullerenes. It is, however, interesting to see what kind of correlations there are between different quantities.
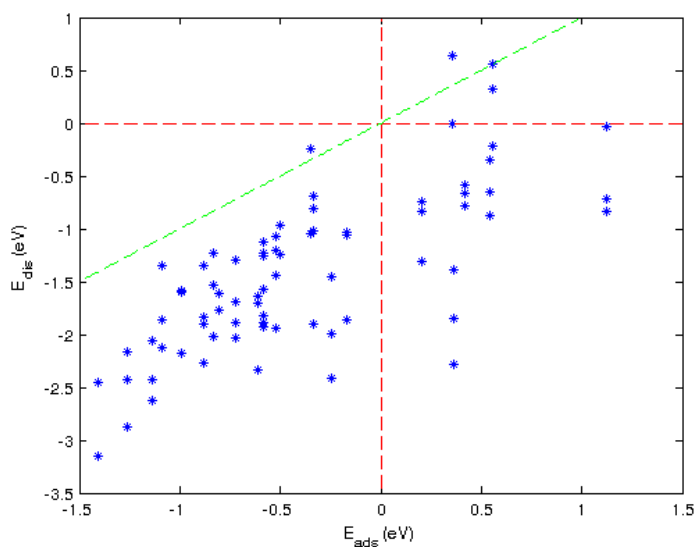

Figure 7.1: Dissociation energies as a function of adsorption energy. Every point corresponds to a dissociation. Red dashed lines mark the zeros in adsorption and dissociation energies. The green dashed line marks when dissociation energy and adsorption energy are equal.

The first question that comes to mind is how the adsorption and dissociation energies are connected. The dissociation energies and adsorption

energies are shown in figure 7.1. We can see that there is some connection between the two energies, but it is hard to say much more than that. We see that there are many different dissociation pathways corresponding to the same adsorption site as is expected. The red dashed lines in figure 7.1 divide the plane in four quadrants. The horizontal red line divides the plane into the upper part, where free oxygen molecule is energetically favourable compared to the dissociated oxygen, and the lower part where dissociation is more favourable. The vertical red dashed line divides the plane into left-hand side, where adsorption is energetically favourable compared to free oxygen molecule, and right-hand side, where it is not. The green dashed line divides the plane into parts where dissociation is energetically favourable compared to adsorption, and a part where adsorption is favourable compared to dissociation.

We see that in most casess dissociation is energetically favourable compared to the adsorption. However, in some cases it is favourable for the oxygen atoms to go from the dissociated configuration to the one, where they form a molecule.

Figure 7.1 tells us something about the different dissociation reactions. However, as the figure only shows the dissociation and adsorption energies, it is quite difficult to see what else is happening. There are more factors changing along each dissociation pathway than the mere energetics. A bit more complete picture of the situation can be obtained when taking into account also the net charge of the system, the presence of nitrogen, and the size of the fullerene. So instead of two-dimensional vector of reaction energies, we now have a five dimensional vector, where a data vector d_i is of the form:

$$d_i = [E_{ads}, E_{dis}, q/atom, N, size], \tag{7.1}$$

where $q/atom$ is the net charge of the system divided by the number of atoms in the system, N is the nitrogen concentration and size is the number of atoms in the fullerene. See appendix B for motivation for this choice of representation. Furthermore, we define a distance for the data vectors as the Euclidean distance between the first two components of the data vectors. It is now possible to make a self-organizing map of the dissociation reaction pathways.

Visualization of the self-organizing map is in figure 7.2. From looking at the U-matrix it is seen that there are two areas with a boundary between them. We see that the adsorption energy is at its highest at the upper side of the map, and at its lowest at the lower side of the map. We see a similar pattern for the dissociation energies. Both dissociation and adsorption energies seem to reach their maximum at the upper right corner. Adsorption en-
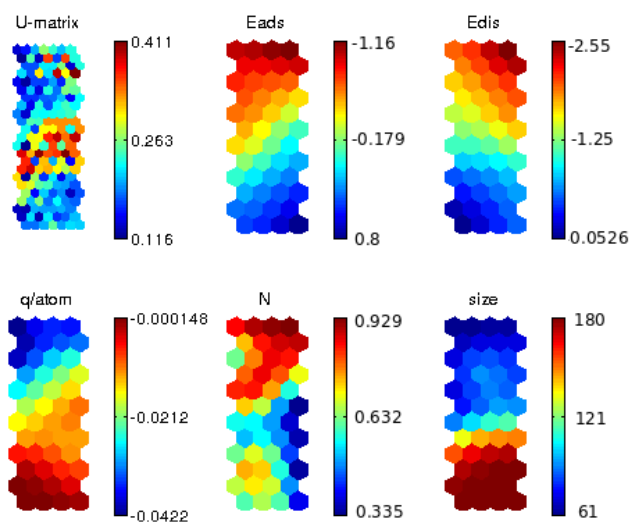
Figure 7.2: The U-matrix and the component planes for the self-organizing map of the dissociation reactions.

ergy reaches its minimum at the lower right corner, whereas the dissociation energy has its minimum at the lower left corner.

Looking at the map we also see a pattern with the charge per atom quantity. We see that the lower side of the map tends to have a low charge per atom, whereas there seems to be more charge per atom on the upper side of the map. The charge has its maximum at the upper left corner of the map, and a minimum at the lower left corner.

We see that the amount of nitrogen also has a distribution. A general pattern seems to be that there is a lot of nitrogen in the upper parts of the map, intermediate values on the lower left side, and small values at the right side. We also see a local minimum at the same place, where there is a global maximum of charge per atom.

We see that the size quantity also has different values at the top and bottom of the map. Upper side of the map has about 60 atoms, and the lower half has about 180 atoms in them. We also see an intermediate range, that seems to correspond to the boundary seen in the U-matrix.

It is quite interesting to see that even if the distance used to train the self-organizing map was based only on adsorption and dissociation energies, there still are clear correlations with the charge per atom, presence of nitrogen and the size of the fullerene.

Table 7.1: Energy barriers for dissociation from HP adsorption site to the sides of a hexagon.

Fullerene	charge	Energy barrier (eV)	E_{ads} (eV)	E_{dis} (eV)
C_{60}	0	0.58	0.36	-1.85
	-1	0.45	-0.24	-1.99
	-3	0.12	-0.99	-2.18
$C_{59}N$	0	0.34	-0.17	-1.86
C_{180}	0	0.63	0.54	-0.65
	-6	0.10	-0.33	-0.69

When thinking about reaction kinetics, it is important to also keep in mind the reaction barriers. Adsorption and dissociation energies alone do not tell the whole story of the reaction. Table 7.1 shows energy barriers for dissociations from HP adsorption site to the sides of the neighbouring hexagon. We can see that adding charge to the system lowers the energy barrier. Furthermore, also adding nitrogen to the fullerene decreases the barrier. We see that the neutral C_{60} and the neutral C_{180} have essentially the same energy barrier, which would indicate that the size does not affect the barrier much.
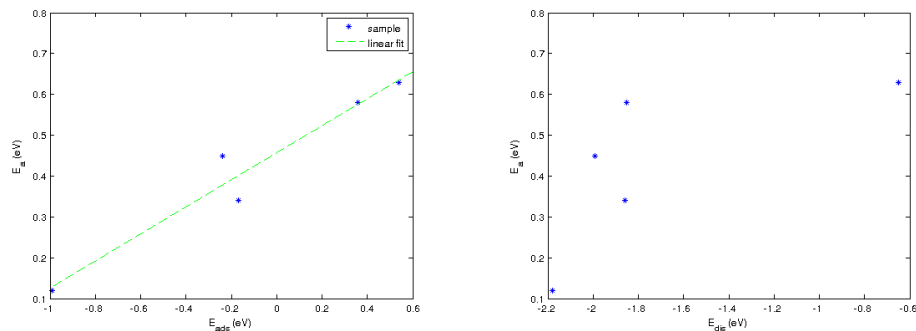
(a) Energy barrier for dissociation as a function of the adsorption energy.

(b) Energy barrier for dissociation as a function of the dissociation energy.

Figure 7.3: Activation energies for dioxygen dissociation.

Energies from table 7.1 are also presented graphically in figure 7.3. We see a general tendency of activation energy increasing with both adsorption energy and dissociation energy. Especially the connection between the adsorption energy and activation energy seems to be almost linear, based on

figure 7.3(a). What should be kept in mind is that every adsorption site has several different dissociation pathways, and every one of them has a different activation energy. Before making fits of activation energy as a function of adsorption energy, it should be made sure that the fit is for the pathway with the lowest activation energy. The same holds for fitting activation and dissociation energies. Even if a final state has a large dissociation energy, that state is not seen in practice if the barrier is very large.

Chapter 8

Discussion

Geometry optimizations for C_{60} and $C_{59}N$ were done with basis sets SZV, DZVP, TZVP, TZV2P, and TZV2PX. The bond lengths did not change after increasing the basis set from DZVP. When dioxygen adsorption geometry optimizations were done with the same basis sets it was seen that the bond lengths did not change after increasing the basis set from TZVP. The optimized geometries were also compared to the ones presented found in literature. Based on the calculations it can be said that DZVP basis set is a large enough a basis set when carbon and nitrogen are present, but when also oxygen is present, TZVP basis set should be used. The bond lenghts calculated with different basis sets are given in appendix A. We see that the calculated bond lenghts are in a relatively good agreement with other calculations [58, 59], and also with experiments [60, 61].

When considering the charge effects on the bond lenghts, as seen in tables 4.1, 4.2, and 4.3, we can say that the effects to the bond lenghts from adding charge to the fullerenes is of the order of picometers. Charge effects on bond lenghts on pristine C_{60} are small. With $C_{59}N$ there seems to be an effect on the HH sites. With pristine C_{180} the bond lenghts on HH1 and HH3 sites increase with charge. Also the bond lenghts on HH2 site decrease with charge.

After the fullerene geometries were optimized it was possible to optimize the geometries for dioxygen adsorption configurations. Adsorption energies for different sites are in tables 5.1, 5.3, 5.4, 5.5, and 5.7. Several trends on the energies are seen: firstly the adsorption energies are more favourable on the smaller fullerenes than on the larger ones. The second thing that is seen is that the presence of nitrogen makes the sites near the nitrogen atom more favourable energetically compared to the pristine fullerene. Adding charge to the system also makes the adsorption energetically more favourable.

The calculated adsorption energies for the pristine fullerenes are similar

to the adsorption energies of oxygen adsorption to carbon nanotubes [62]. Ref. [63] calculated oxygen adsorption energies 0.25 eV for the HH site, and 1.06 eV for the HP site at the cap of a (5,5) carbon nanotube. The difference in the adsorption energies for these two sites found on the literature is 0.81 eV, which is of the same magnitude as the difference of 0.71 eV which was obtained in this study for adsorption on C_{60}. It can therefore be said that there is a definite site dependence in the reaction energies.

Tables 6.1, 6.2, 6.3, and 6.4 show the dissociation energies for different dissociation pathways. Comparing tables 6.3 and 6.4 gives us an estimate on the range in which the nitrogen atom has an effect. When the oxygen atoms move from HH3 site towards the nitrogen atom, the dissociation is energetically more favourable than when the oxygen atoms move away from the nitrogen atom. Furthermore when the oxygen atoms move away from the nitrogen atom, the result is energetically the same as in the case of symmetric dissociation from the HH3 site of the pristine C_{180}. It is therefore possible to say that the effects of the nitrogen in C_{180} are limited to the polygons the nitrogen atom is located in. When considering dissociation pathways on C_{60} and $C_{59}N$ as seen in tables 6.1 and 6.2 leads to the same conclusion about the effects of nitrogen on C_{60}, at least for small charges. With pristine C_{60} the oxygen atoms dissociated in a pentagon formed chain-like structures with carbon atoms with small charges, and epoxy structures with larger charges. $C_{59}N$ forms chain-like structures even with larger charges.

Figure 7.1 shows the correspondence between the adsorption energy and the dissociation energy for different pathways and fullerenes. There is some correlation between the two energies. The Pearson correlation coefficient between them is 0.76 and the coefficient of determination is 0.58. This means that the linear correlation between the adsorption and dissociation energy is moderate or strong [64]. Similar linear relationships between free energies have been documented before [65, 66].

Figure 7.2 is very interesting, because it shows that even when the self-organizing map is trained only with the data of the adsorption and dissociation energies, there is also a clear structure in the charge per atom, presence of nitrogen, and the size of the fullerene component planes. Based on the map it is possible to say, at least qualitatively, that adding charge or nitrogen to a fullerene system makes adsorption and dissociation energetically more favourable, and that increasing the size of the fullerene makes adsorption and dissociation energetically less favourable.

Table 7.1 and figure 7.3 show the energy barrier for the dissociation, the adsorption energy, and the dissociation for several dissociation pathways. It seems clear that adding charge or nitrogen to the system makes the energy barrier for the dissociation lower. It would also seem that the size of the fullerene does not affect the barrier for dissociation very much. The difference in the barrier height for a similar dissociation on C_{60} and C_{180} is only 0.05 eV. This can be compared to the fact that a single extra electron on C_{60} makes the same barrier lower by 0.13 eV, or to the addition of a nitrogen atom, which lowers the barrier by 0.24 eV. This comparison would indicate that the size effects on the barrier are smaller than those of the charge or nitrogen.

Based on figure 7.3(a) it would seem that there is a strong linear correlation between the adsorption energy and the energy barrier for the dissociation. The correlation coefficient between them is 0.97, and the coefficient of determination is 0.95. However, it should be kept in mind that there are not very many samples for the energy barriers. As there are only five data points, the risk of overfitting must be acknowledged. It should also be kept in mind that every adsorption site has several possible dissociation pathways, all of which have their own energy barriers. It is therefore important to be very careful when fitting these linear models. In practice, the most interesting relationship is between the adsorption energy and the lowest activation energy for dissociation.

A good topic for future research could be investigating the relationship between the adsorption energy of an adsorption site and the lowest energy barrier for different dissociation pathways from that site. Having a better knowledge of the relationships between different system parameters would make engineering the fullerene systems with the optimal properties for a given task easier. Keeping up with that line of inquiry, it would also be interesting to see what is the dissociation pathway with the lowest energy barrier for a given site. A plausible guess would be that for near-neutral fullerenes the pathways with lowest barriers would be the symmetric ones, and for more charged fullerenes the asymmetric dissociation pathways.

Having more data on the energy barriers for different pathways could also be used as input for a self-organizing map. In this thesis the reaction energies were used in the distance function. If the activation energies were also available for every reaction path, the component planes of the map could show more accurately what exactly is going on. In practice this would require a relatively large number of NEB calculations. However, this might currently not be the best use of computational resources.

When a NEB calculation is run between two energy minimum configurations and there is a minimum energy configuration on the reaction pathway, this can lead to problems with convergence of calculation. This practical aspect should always be kept in mind when doing NEB calculations.

Chapter 9

Conclusions

Four different fullerenes with different charges were studied in this thesis: fullerenes C_{60} and C_{180} in both pristine and nitrogen substituted form. Every studied fullerene was further studied with several different charges.

Density functional calculations about adsorption and dissociation of dioxygen molecules on the fullerenes were made. It was concluded that negative charge and nitrogen doping both make the adsorption and the dissociation of the oxygen molecules on fullerenes energetically more favourable. We also see that increasing the size of the fullerenes makes both the adsorption and dissociation energetically less favourable. A number of adsorption and dissociation energies were calculated, so the conclusions about them are rather reliable.

It was also seen that the adsorption and dissociation energies had a rather strong dependence on the site considered. The site dependence observed in this thesis was in line with those found in the literature.

It was also concluded that both extra charge and nitrogen doping lower the energy barrier for the dissociation reaction for the dioxygen molecule. It was seen that the dissociation barrier is only weakly dependent on the size of the fullerene. A relatively small number of activation energies were calculated, limiting the reliability of the conclusions compared to those made about the adsorption and dissociation energies.

Besides these observations, it was also seen that when extra charge is brought to a fullerene system, it spreads out nearly evenly among all the atoms. This is true also in the cases where there is oxygen present on the fullerene.

These observations indicate that charged fullerenes remain a promising catalyst for future applications in oxygen reduction reactions. For future applications in catalysis it is important to find suitable combinations of the relevant reaction energies and energy barriers. The findings in this thesis show that adding charge and nitrogen doping, or taking a fullerene of different size all change these energies.

Bibliography

[1] Margaret A. Gabriel, Thierry Deutsch, and Alejandro A. Franco. Fullerene-based materials as catalysts for fuel cells. *ECS Transactions*, 25(22):1–6, 2010.

[2] James Larminie, Andrew Dicks, and Maurice S McDonald. *Fuel cell systems explained*, volume 2. Wiley Chichester, 2003.

[3] Rainer Kujala. Dioxygen adsorption on nitrogen defects in carbon nanotubes - a computational study, 2010.
Bachelor's thesis, Aalto University.
`http://urn.fi/URN:NBN:fi:aalto-201305164972`.

[4] J. K. Nørskov, J. Rossmeisl, A. Logadottir, L. Lindqvist, J. R. Kitchin, T. Bligaard, and H. Jónsson. Origin of the overpotential for oxygen reduction at a fuel-cell cathode. *The Journal of Physical Chemistry B*, 108(46):17886–17892, 2004.

[5] K. Broka and P. Ekdunge. Modelling the pem fuel cell cathode. *Journal of Applied Electrochemistry*, 27(3):281–289, 1997.

[6] Kuanping Gong, Feng Du, Zhenhai Xia, Michael Durstock, and Liming Dai. Nitrogen-doped carbon nanotube arrays with high electrocatalytic activity for oxygen reduction. *Science*, 323(5915):760–764, 2009.

[7] CE Banks, GG Wildgoose, CGR Heald, and RG Compton. Oxygen reduction catalysis at anthraquinone centres molecularly wired via carbon nanotubes. *Journal of the Iranian Chemical Society*, 2(1):60–64, 2005.

[8] International Union of Pure and Applied Chemistry. *IUPAC Gold Book*. IUPAC, 2006.

[9] Boy Cornils and Wolfgang A. Herrmann. Concepts in homogeneous catalysis: the industrial view. *Journal of Catalysis*, 216(1-2):23 – 31, 2003. 40th Anniversary Commemorative Issue.

[10] Noritaka Mizuno and Makoto Misono. Heterogeneous catalysis. *Chemical Reviews*, 98(1):199–218, 1998.

[11] Keith J. Laidler. The development of the arrhenius equation. *Journal of Chemical Education*, 61(6):494, 1984.

[12] Peter Hänggi, Peter Talkner, and Michal Borkovec. Reaction-rate theory: fifty years after kramers. *Rev. Mod. Phys.*, 62:251–341, Apr 1990.

[13] Matt Petrowsky and Roger Frech. Temperature dependence of ion transport: The compensated arrhenius equation. *The Journal of Physical Chemistry B*, 113(17):5996–6000, 2009. PMID: 19338318.

[14] R. Kirchheim and X. Y. Huang. A relationship between prefactor and activation energy for diffusion. *physica status solidi (b)*, 144(1):253–257, 1987.

[15] F.J.M. Horn and J.E. Bailey. An application of the theorem of relaxed control to the problem of increasing catalyst selectivity. *Journal of Optimization Theory and Applications*, 2(6):441–449, 1968.

[16] Rod Borup, Jeremy Meyers, Bryan Pivovar, Yu Seung Kim, Rangachary Mukundan, Nancy Garland, Deborah Myers, Mahlon Wilson, Fernando Garzon, David Wood, et al. Scientific aspects of polymer electrolyte fuel cell durability and degradation. *Chemical reviews*, 107(10):3904–3951, 2007.

[17] S. Dresselhaus, G. Dresselhaus, and P.C. Eklund. *Science of Fullerenes and Carbon Nanotubes: Their Properties and Applications*. Elsevier Science, 1996.

[18] H. W. Kroto, J. R. Heath, S. C. O'Brien, R. F. Curl, and R. E. Smalley. C60: Buckminsterfullerene. *Nature*, 318(6042):162–163, November 1985.

[19] P.W. Fowler and D.E. Manolopoulos. *An atlas of fullerenes*. International series of monographs on chemistry. Clarendon Press, 1995.

[20] Kaiyuan Li, Gyula Eres, Jane Howe, Yen-Jun Chuang, Xufan Li, Zhanjun Gu, Litong Zhang, Sishen Xie, and Zhengwei Pan. Self-assembly of graphene on carbon nanotube surfaces. *Scientific reports*, 3, 2013.

[21] Mitsutaka Fujita, Riichiro Saito, G. Dresselhaus, and M. S. Dresselhaus. Formation of general fullerenes by their projection on a honeycomb lattice. *Phys. Rev. B*, 45:13834–13836, Jun 1992.

[22] Charles M. Lieber and Chia-Chun Chen. Preparation of fullerenes and fullerene-based materials. volume 48 of *Solid State Physics*, pages 109 – 148. Academic Press, 1994.

[23] Iris Lamparth, Berthold Nuber, Georg Schick, Andreas Skiebe, Thomas Grösser, and Andreas Hirsch. C59n+ and c69n+: Isoelectronic heteroanalogues of c60 and c70. *Angewandte Chemie International Edition in English*, 34(20):2257–2259, 1995.

[24] Otto Vostrowsky and Andreas Hirsch. Heterofullerenes. *Chemical Reviews*, 106(12):5191–5207, 2006.

[25] H.-J. Muhr, R. Nesper, B. Schnyder, and R. Kötz. The boron heterofullerenes {C59B} and c69b: generation, extraction, mass spectrometric and {XPS} characterization. *Chemical Physics Letters*, 249(5-6):399 – 405, 1996.

[26] Tsutomu Ohtsuki, Kaoru Ohno, Keiichiro Shiga, Yoshiyuki Kawazoe, Yutaka Maruyama, and Kazuyoshi Masumoto. Formation of as- and ge-doped heterofullerenes. *Phys. Rev. B*, 60:1531–1534, Jul 1999.

[27] M. Pellarin, C. Ray, J. Lermé, J. L. Vialle, M. Broyer, X. Blase, P. Kéghélian, P. Mélinon, and A. Perez. Photolysis experiments on sic mixed clusters: From silicon carbide clusters to silicon-doped fullerenes. *The Journal of Chemical Physics*, 110(14):6927–6938, 1999.

[28] I.M.L. Billas, W. Branz, N. Malinowski, F. Tast, M. Heinebrodt, T.P. Martin, C. Massobrio, M. Boero, and M. Parrinello. Experimental and computational studies of heterofullerenes. *Nanostructured Materials*, 12(5-8):1071 – 1076, 1999. The Fourth International Conference on Nanostructured Materials (NANO '98).

[29] H Shinohara. Endohedral metallofullerenes. *Reports on Progress in Physics*, 63(6):843, 2000.

[30] Michele Pavanello, Abraham F. Jalbout, Bartosz Trzaskowski, and Ludwik Adamowicz. Fullerene as an electron buffer: Charge transfer in li@c60. *Chemical Physics Letters*, 442(4-6):339 – 343, 2007.

[31] Bharat Bhushan, B. K. Gupta, Garrett W. Van Cleef, Cynthia Capp, and James V. Coe. Fullerene (c60) films for solid lubrication. *Tribology Transactions*, 36(4):573–580, 1993.

[32] L. Rapoport, N. Fleischer, and R. Tenne. Fullerene-like ws2 nanoparticles: Superior lubricants for harsh conditions. *Advanced Materials*, 15(7-8):651–655, 2003.

[33] L. Rapoport, O. Nepomnyashchy, A. Verdyan, R. Popovitz-Biro, Y. Volovik, B. Ittah, and R. Tenne. Polymer nanocomposites with fullerene-like solid lubricant. *Advanced Engineering Materials*, 6(1-2):44–48, 2004.

[34] B.K. Gupta and B. Bhushan. Fullerence particles as an additive to liquid lubricants and greases for low friction and wear. *Lubrication Engineering*, Jul 1994.

[35] Gareth A. Hughes. Nanostructure-mediated drug delivery. *Nanomedicine: Nanotechnology, Biology and Medicine*, 1(1):22 – 30, 2005.

[36] Rajesh Singh and James W. Lillard Jr. Nanoparticle-based targeted drug delivery. *Experimental and Molecular Pathology*, 86(3):215 – 223, 2009. Special Issue: Structural Biology.

[37] Barbara Haley and Eugene Frenkel. Nanoparticles for drug delivery in cancer treatment. *Urologic Oncology: Seminars and Original Investigations*, 26(1):57 – 64, 2008. The Potential of Nanotechnology in Urologic Oncology.

[38] Marco Gallo, Alejandra Favila, and Daniel Glossman-Mitnik. Dft studies of functionalized carbon nanotubes and fullerenes as nanovectors for drug delivery of antitubercular compounds. *Chemical Physics Letters*, 447(1-3):105 – 109, 2007.

[39] A.Ya. Vul, V.M. Davidenko, S.V. Kidalov, S.S. Ordanyan, and V.A. Yashin. Fullerenes catalyze the graphite-diamond phase transition. *Technical Physics Letters*, 27(5):384–386, 2001.

[40] Anton W. Jensen and Coreen Daniels. Fullerene-coated beads as reusable catalysts. *The Journal of Organic Chemistry*, 68(2):207–210, 2003.

[41] V.M. Davidenko, S.V. Kidalov, F.M. Shakhov, M.A. Yagovkina, V.A. Yashin, and A.Ya. Vul. Fullerenes as a co-catalyst for high pressure - high temperature synthesis of diamonds. *Diamond and Related Materials*, 13(11-12):2203 – 2206, 2004. Proceedings of the 9th International Conference on New Diamond Science and Technology (ICNDST-9).

[42] Nataliya F. Goldshleger. Fullerenes and fullerene-based materials in catalysis. *Fullerene Science and Technology*, 9(3):255–280, 2001.

[43] Junjie GUO, Xiaowei YANG, Yanli YAO, Xiaomin WANG, Xuguang LIU, and Bingshe XU. Pt/onion-like fullerenes as catalyst for direct methanol fuel cell. *Rare Metals*, 25(6, Supplement 1):305 – 308, 2006.

[44] Roberto Pellicciari, Benedetto Natalini, Tatiana V. Potolokova (nee Mukha), Maura Marinozzi, Marina N. Nefedova, Alexander S. Peregudov, and Viatcheslav I. Sokolov. Thermal and catalytic reactions of diazoacetylmetallocenes with [60]fullerene. *Synthetic Communications*, 33(6):903–914, 2003.

[45] W. Kohn, A. D. Becke, and R. G. Parr. Density functional theory of electronic structure. *The Journal of Physical Chemistry*, 100(31):12974–12980, 1996.

[46] Joost VandeVondele, Matthias Krack, Fawzi Mohamed, Michele Parrinello, Thomas Chassaing, and Jürg Hutter. Quickstep: Fast and accurate density functional calculations using a mixed gaussian and plane waves approach. *Computer Physics Communications*, 167(2):103 – 128, 2005.

[47] John P. Perdew, Kieron Burke, and Matthias Ernzerhof. Generalized gradient approximation made simple. *Phys. Rev. Lett.*, 77:3865–3868, Oct 1996.

[48] S. Goedecker, M. Teter, and J. Hutter. Separable dual-space gaussian pseudopotentials. *Phys. Rev. B*, 54:1703–1710, Jul 1996.

[49] C. Hartwigsen, S. Goedecker, and J. Hutter. Relativistic separable dual-space gaussian pseudopotentials from h to rn. *Phys. Rev. B*, 58:3641–3662, Aug 1998.

[50] M. Krack. Pseudopotentials for h to kr optimized for gradient-corrected exchange-correlation functionals. *Theoretical Chemistry Accounts*, 114(1-3):145–152, 2005.

[51] Daniel Sheppard, Rye Terrell, and Graeme Henkelman. Optimization methods for finding minimum energy paths. *The Journal of Chemical Physics*, 128(13):134106, 2008.

[52] Hannes Jonsson, Greg Mills, and Karsten W Jacobsen. Nudged elastic band method for finding minimum energy paths of transitions. 1998.

[53] Shalom Srebrenik, Richard F. W. Bader, and T. Tung Nguyen-Dang. Subspace quantum mechanics and the variational principle. *The Journal of Chemical Physics*, 68(8):3667–3679, 1978.

[54] R. F. W. Bader. Quantum topology of molecular charge distributions. iii. the mechanics of an atom in a molecule. *The Journal of Chemical Physics*, 73(6), 1980.

[55] Teuvo Kohonen. *Self-organizing maps*, volume 30. Springer, 2001.

[56] T. Kohonen. The self-organizing map. *Proceedings of the IEEE*, 78(9):1464–1480, 1990.

[57] Teuvo Kohonen. The self-organizing map. *Neurocomputing*, 21(1-3):1 – 6, 1998.

[58] Feng Gao, Guang-Lin Zhao, Shizhong Yang, and James J. Spivey. Nitrogen-doped fullerene as a potential catalyst for hydrogen fuel cells. *Journal of the American Chemical Society*, 135(9):3315–3318, 2013.

[59] Neeraj Misra, Apoorva Dwivedi, and Anoop Pandey. Geometrical electronic, and vibrational properties of fullerene rings doped with transition metals. *Chinese Journal of Physics*, 50(1):64–72, 2012.

[60] Kenneth Hedberg, Lise Hedberg, Donald S Bethune, CA Brown, HC Dorn, Robert D Johnson, and M De Vries. Bond lengths in free molecules of buckminsterfullerene, c60, from gas-phase electron diffraction. *Science*, 254(5030):410–412, 1991.

[61] CS Yannoni, PP Bernier, DS Bethune, G Meijer, and JR Salem. Nmr determination of the bond lengths in c60. *Journal of the American Chemical Society*, 113(8):3190–3192, 1991.

[62] Jijun Zhao, Alper Buldum, Jie Han, and Jian Ping Lu. Gas molecule adsorption in carbon nanotubes and nanotube bundles. *Nanotechnology*, 13(2):195, 2002.

[63] Chang-Youn Moon, Yong-Sung Kim, Eun-Cheol Lee, Young-Gu Jin, and K. J. Chang. Mechanism for oxidative etching in carbon nanotubes. *Phys. Rev. B*, 65:155401, Mar 2002.

[64] Kelly H. Zou, Kemal Tuncali, and Stuart G. Silverman. Correlation and simple linear regression. *Radiology*, 227(3):617–628, 2003. PMID: 12773666.

[65] David Loffreda, Françoise Delbecq, Fabienne Vigné, and Philippe Sautet. Fast prediction of selectivity in heterogeneous catalysis from extended brønsted-evans-polanyi relations: A theoretical insight. *Angewandte Chemie International Edition*, 48(47):8978–8980, 2009.

[66] Ziyun Wang, Bo Yang, Yulong Wang, Yifang Zhao, X.-M. Cao, and P. Hu. Identifying the trend of reactivity for sp2 materials: an electron delocalization model from first principles calculations. *Phys. Chem. Chem. Phys.*, 15:9498–9502, 2013.

Appendix A

Basis set test results

Table A.1: Table of calculated bond lengths of $C_{59}N$. Comparison is done with ref [58]. Unit is Å.

site	Gao et al.	DZVP	TZVP	TZV2P	TZV2PX
HP-Pauling	1.41	1.43	1.43	1.43	1.43
HH-Pauling	1.38	1.40	1.40	1.40	1.40
HP-CC	1.42	1.44	1.44	1.44	1.44
HH-CC	1.38	1.39	1.39	1.39	1.39
short bridge	2.28	2.23	2.30	2.30	2.30
long bridge	2.41	2.44	2.44	2.44	2.44

Table A.2: Calculated bond lengths at the HH Pauling adsorption site of $C_{59}N$. Comparison is done with ref [58]. Unit is Å.

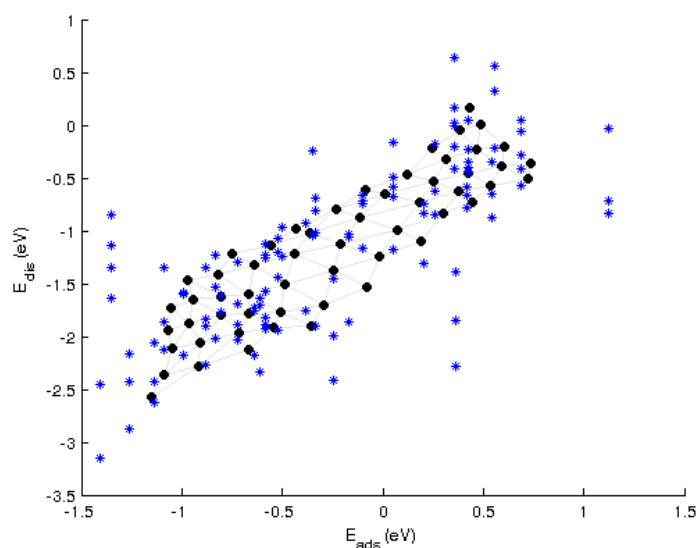| source	d_{C-O} (Å)	d_{O-O} (Å)
Gao et al.	1.57	1.30
DZVP	1.58	1.32
TZVP	1.73	1.29
TZV2P	1.73	1.29
TZV2PX	1.73	1.29

Appendix B

SOM figures

Figure B.1:   The calculated adsorption and dissociation energies are on blue. Black circles are the adsorption energy and dissociation energy of the codebook vectors. Gray line segments show the nearest neighbour relations between the neurons of the map. Compare to figures 7.1 and 7.2.
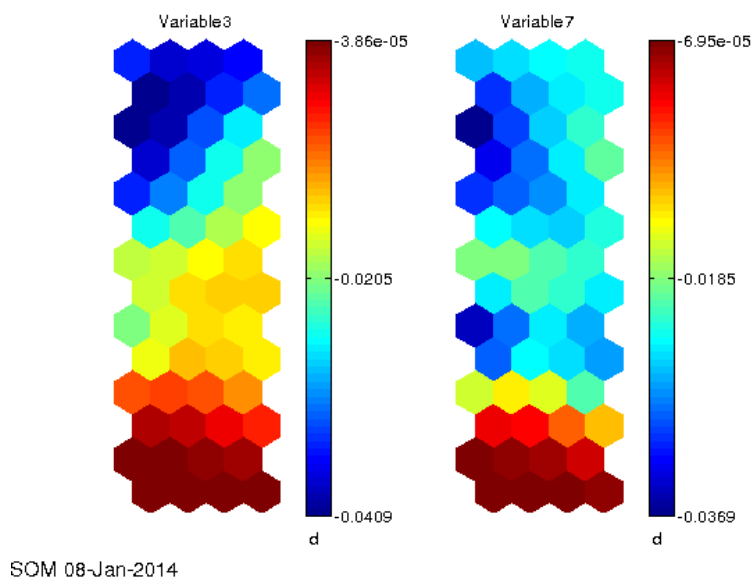
Figure B.2: Component planes for charge per atom and total charge. We see that the charge per atom is more interesting quantity of these two.
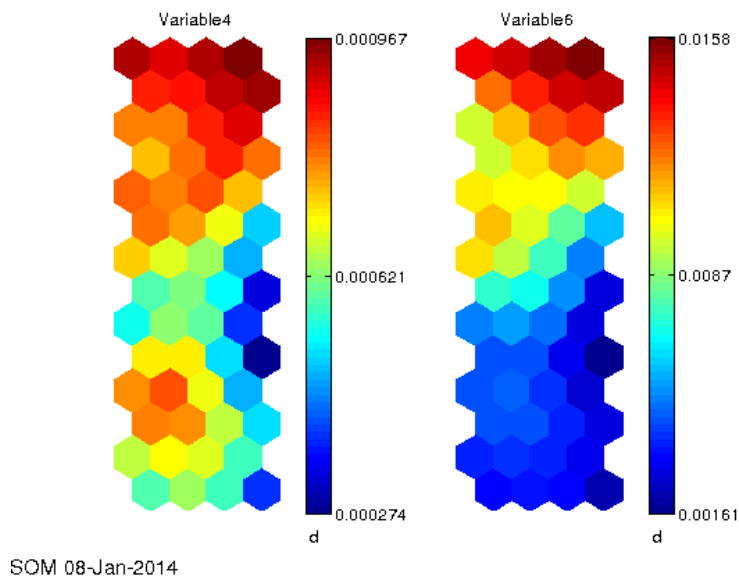

Figure B.3: Component planes for presence of nitrogen and the nitrogen per atom. We see that using the presence of nitrogen as a binary variable is more informative than using the nitrogen concentration.
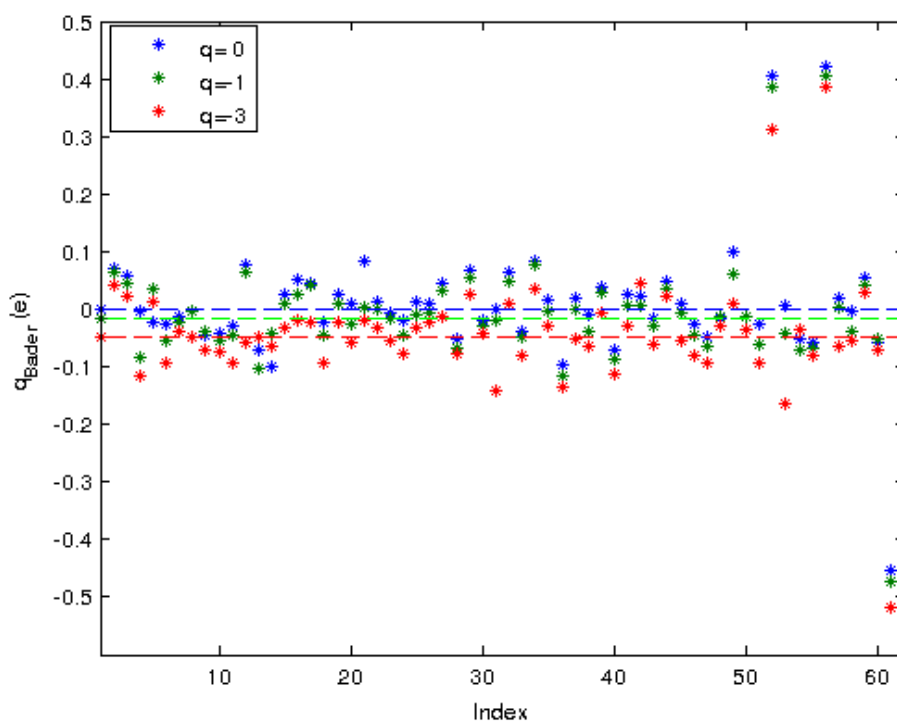
Appendix C

Bader charge figures

Figure C.1: Bader charges for the HP adsorption site of the C_{60}. Atoms 1 to 60 are carbons, atoms 61 and 62 are oxygens. In table 5.2, atom 51 is C(1), 56 is C(2), 61 is O(1), and 62 is O(2). Dashed lines show what the Bader charge would be, were the charge evenly distributed among the atoms.
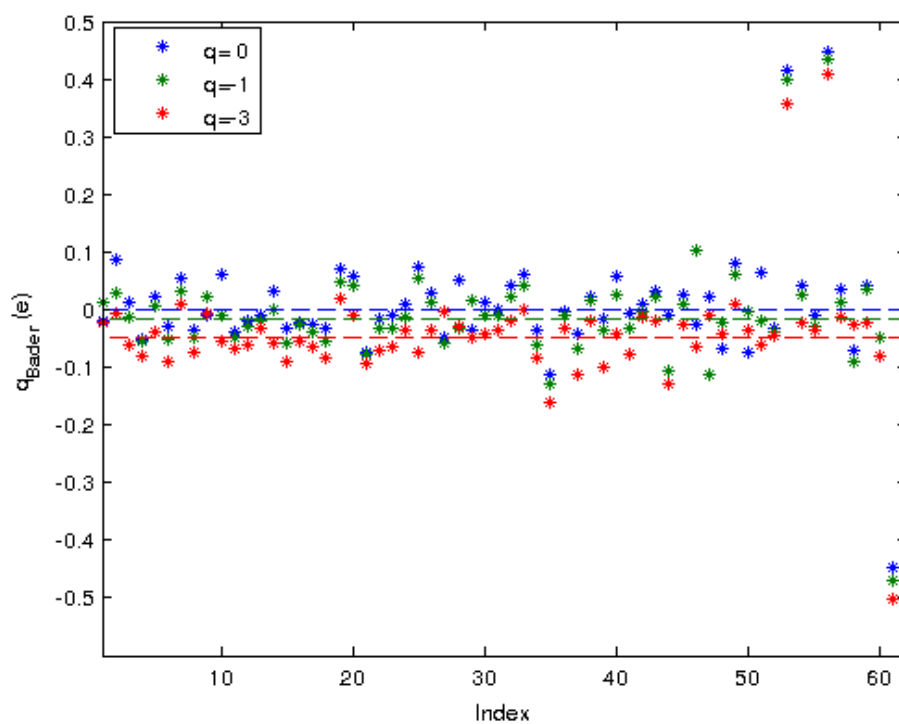
Figure C.2: Bader charges for the HH adsorption site of the C_{60}. Atoms 1 to 60 are carbons, atoms 61 and 62 are oxygens. In table 5.2, atom 53 is C(1), 56 is C(2), 61 is O(1), and 62 is O(2). Dashed lines show what the Bader charge would be, were the charge evenly distributed among the atoms.